AD-A070 757 LAMONT-DOHERTY GEOLOGICAL OBSERVATORY PALISADES N Y F/G 8/10
A REFRACTION EXPERIMENT USING OCEAN BOTTOM SEISMOGRAPHS AND IM--ETC(U)
SEP 78 H ROWLETT, K MCCAMY, P J FOX N00014-76-C-0818

UNCLASSIFIED NL

| OF |
AD
A070757

END
DATE
FILMED
8-79
DDC

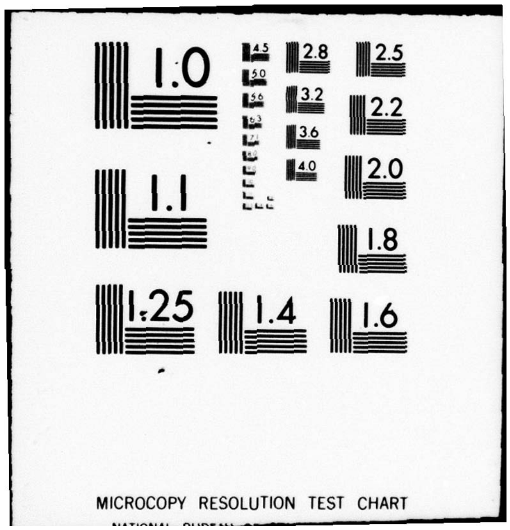
1.0
1.1
1.25
1.4
1.6
1.8
2.0
2.2
2.5
2.8
3.2
3.6
4.0
MICROCOPY RESOLUTION TEST CHART

LEVEL II

A REFRACTION EXPERIMENT USING OCEAN BOTTOM SEISMOGRAPHS AND IMPLICATIONS OF A STRUCTURAL MODEL OF THE CREST OF THE MID-ATLANTIC RIDGE AT ~~37°N~~ 37 deg N

Hugh Rowlett[1] Keith McCamy Paul J. Fox[2]

Lamont-Doherty Geological Observatory of Columbia University

Palisades, New York 10964

and

Paul J. Fox

Department of Geological Sciences

State University of New York at Albany

Albany, New York 12222

Contract No. N00014-76-C-0818
Date: Sept. 1978

ABSTRACT

Eight seismic refraction lines were shot along different azimuths away from two ocean bottom seismographs located between Deep Sea Drilling Project holes 332 and 333 in the crestal mountains west of the median valley of the mid-Atlantic ridge near 37°N. Large variations, 5.6 to 6.6 km/sec, were observed in the apparent velocities from a main refractor that is approximately 1.7 km beneath the seafloor at the receivers. The variation of the apparent velocities of the main refractor is not explained by a simple flat-layered model or any other systematic cause, suggesting tectonic control of the velo-

---

[1] Lamont-Doherty Geological Observatory Contribution Number 0000.

[2] Also, Department of Geological Sciences, Columbia University.

city structure. The compressional velocity for the main refractor is about 6.3 km/sec. A study of travel-time residuals of the main refractor from refraction lines perpendicular to the median valley and local structural trends on the sea floor suggests that the block faulting that causes the relief of the sea floor may extend to the depth of the main refractor. Travel-time data from split profiles suggest that the depth of the main refractor in the crestal mountains increases away from the median valley. A structural model, based on results from this experiment and two refraction experiments conducted by others within 30 km of this experiment, is proposed for the mid-Atlantic ridge at 37°N. The model suggests that a difference in depth exists between material of similar velocity beneath the inner floor of the median valley and the crestal mountains. The difference in depth increases away from the axis of the median valley over a distance of 10 to 15 km and decays in the crestal mountains. Material of a similar velocity is at approximately the same depth beneath the sea floor in both the inner floor of the median valley and the crestal mountains. This constant thickness for the upper portion of the crust suggests that the zone of crustal accretion for the upper ∿2 km is restricted to the inner floor. The proposed structural model also supports hypotheses based on morphological observations at 37°N that relief between the floor of the median valley and crestal mountains is controlled by block faulting. Large travel-time residuals, from a refraction line shot near the oldest section of fracture zone A (western limb), show that strong heterogeneity exists in the crust over a few kilometers, and imply that portions of the crust of the fracture

zone may have a significantly higher average velocity than oceanic crust outside of the fracture zone.

INTRODUCTION

A main goal of marine seismology is to measure seismic velocities to constrain petrologic and structural models of the ocean crust. This is especially important for models of the lower crust which has not yet been reached by drilling and cannot be directly examined. Although recent compilations of marine refraction work [Raitt, 1963; Shor et al., 1970; Houtz and Ewing, 1976] show histograms of velocity measurements whose peaks grossly characterize most of the oceanic crust, velocity structures near ridge crests are still unclear. There have been several seismic measurements near the ridge crest in the North Atlantic [LePichon et al., 1965; Keen and Tramontini, 1970; Talwani et al., 1971; Fowler and Matthews, 1974; Fowler, 1976; Poehls, 1974; Laughton, unpublished manuscript, 1974; Whitmarsh, 1973, 1975, 1978]. Even though most of these studies (those published since 1973) were clustered within 30 to 40 km of one another in the FAMOUS area near "rift valley 2" at 37°N, there is considerable disparity between the observed velocities and the inferred crustal models. Structurally induced relief of igneous stratigraphy or other lateral heterogeneities, inadequate data and misinterpretation are likely causes of the disagreement between these studies. This paper describes the results of a refraction experiment that investigates the discrepancies of previous work in the crestal mountains at 37°N. We also compare the results of our refraction experiment with the other refraction experiments conducted in the median valley at 37°N and propose a structural model for the upper 3 km of oceanic crust at 37°N based on the better constrained experiments.

Whitmarsh [1975] and Fowler [1976] present structural models for the oceanic crust near the median valley at 37°N. The model proposed here is based in part on some of their observations. The main difference between our model and previous models at 37°N is that we include results from refraction profiles that were confined to the crestal mountains.

THE REFRACTION EXPERIMENT

This experiment was conducted during VEMA 32-03 in the western crestal mountains of the FAMOUS area of the mid-Atlantic ridge at 37°N. Figure 1 shows the location of three bottom seismographs with respect to the median valley, the shooting track, and the locations of holes 332 and 333 of the Deep Sea Drilling Project. Our intent was to have a triangular array of receivers at the center of the shooting pattern so we could measure apparent velocities and apparent azimuths of the signals from the shots to help separate the effects of heterogeneities in the crust at the source and receiver. Unfortunately, OBS 3 failed to record satisfactorily, and the other two, through an unavoidable error in navigation, were placed too close together to be useful for this purpose. Nevertheless, the radial shooting tracks (numbered in Figure 1) do permit us to evaluate the effect of azimuth on the apparent velocities and, using certain assumptions, to determine the actual velocity of the major refracted arrivals.

The ocean bottom seismographs [McDonald et al., 1977] directly record sound waves in the water, horizontal and vertical ground motion, and a precise time code onto magnetic tape. The seismic pass-band

(3 db points) is from 8 to 60 Hz, suitable for both detailed seismic refraction and microearthquake experiments.

Tetrytol was used as a sound source with charge size ranging from the equivalent of 1.59 to 2.95 kg TNT. At ranges less than 12 km from the array of instruments shots were spaced at 0.5 km to obtain adequate coverage of refractions. Shots were spaced 1.0 km on the average for ranges greater than 12 km from the array center. Satellite navigation was adequate for deployment and recovery of the instruments and for dead reckoning the shot lines along major bathymetric features. Since we altered course along the shooting track several times, satellite navigation was, however, inadequate for calculating the range between the shots and the receivers. Instead, the travel-times of the direct water waves were used for ranging.

An average water velocity of 1.495 km/sec was used to calculate the shot to receiver ranges. Ranges calculated using this water velocity were within $\pm$ 30 m of those calculated from a velocity-depth model of the water column derived from expendable bathy-thermograph drops and velocity data [P. J. Bucca, personal communication, 1975] of the Naval Oceanographic Office.

INTERPRETATION

Kennett and Orcutt [1976] discuss the problems in marine geophysics associated with the assumption of layers with uniform velocities or continuously varying velocity gradients as the velocity-depth function. Orcutt et al. [1976] and Helmberger and Morris [1969] present models of the upper oceanic crust, using both travel-time

and amplitude data, that suggest that strong velocity gradients exist in the upper oceanic crust. Whitmarsh [1978], using travel-time data from a refraction profile in the immediate vicinity of our experiment and several other refraction profiles located in the North Atlantic, concludes that the seismic evidence favors only models with velocity gradients in the upper 2 km of the oceanic crust.

Inversions of travel-time data for models with velocity gradients assume lateral homogeneity. This assumption may be adequate for refraction profiles nearly parallel to local structural trends. On the other hand, only reversed travel-time data, fitted by ray tracing, can adequately describe models with velocity gradients that vary laterally. Analysis of the apparent velocities of arrivals from the unreversed, radial profiles of our experiment, as discussed later, show that the apparent velocities of arrivals at similar ranges vary significantly. The variation in apparent velocities strongly suggest that a laterally homogeneous model does not generally apply in all directions from the OBS's. To compare the travel-time data from all of the refraction profiles we choose for simplicity dipping layers to describe the gross velocity structure of the area. The data cannot uniquely constrain a more realistic model characterized by a general and continuous variation of velocity.

Record Section

In Figure 2 we present a record section of seismograms recorded on the hydrophone channel of OBS 1 from shots fired along line 4. The main features of the record section of line 4 are common to all of

the radial refraction lines of this experiment. Seismograms of the record section are hand-digitized about one second before the first arrival to the arrival time of the direct water-wave. The amplitudes of the seismograms of the record section are not corrected for shot size or range. The record section is corrected for an OBS on a datum with a water layer of 2.5 km and surface shots.

The record section of Figure 2 shows that first arrivals are easily detected, especially at ranges less than about 13 km. For ranges greater than about 13 km, first arrivals for several of the shots are emergent, even though the shot sizes were constant at these ranges. There is considerable variation in the amplitudes of first arrivals at ranges greater than about 8 km. There is also significant, late energy after the first arrival for ranges less than 8 km. For ranges of 12 km and greater, the first two seconds of the seismograms are characterized solely by the first arrival and its multiple and, the seismogram appears less complicated. Qualitatively, we interpret this changing complexity of the signal with range by a more intense scattering of energy along propagation paths in the uppermost crust compared with energy propagating deeper in the crust.

One important feature of the record section is that second arrivals, interpreted as compressional waves refracted or reflected within the crust, are not observable. (This excludes multiples. Shear and converted shear waves are, of course, observed as second arrivals and are discussed later.) The lack of second arrivals suggests that velocity gradients are present in the crust [Kennett and Orcutt, 1976; Whitmarsh, 1978]. In fact, the relatively large amplitudes of first arrivals at small ranges in Figure 2 are in agreement with a strong

velocity gradient in the upper crust [Kennett and Orcutt, 1976]. Refractions from the uppermost portion of the crust appear as first arrivals for a relatively short interval of range along 8 of the 13 lines recorded by the OBS's (about 3 km for most of the lines). Minimum ranges for 5 of the remaining lines are too great to record these refractions. Thus, it is difficult to resolve the detailed velocity structure of the uppermost crust.

Nonetheless, examination of the record section in Figure 2 shows that the gross velocity structure can be approximated by a two refractor model. Therefore, we choose to represent the upper portion of the crust as a single layer and designate refractions from this layer as P_2 arrivals. First arrivals with ranges greater than about 6 km are also treated as propagating along one refractor (the main refractor). These arrivals are designated as P_3 arrivals in this paper.

Schematic time-distance data, representing the actual data of this experiment, and a ray-path diagram of refracted phases observed during this experiment, are illustrated in Figure 3. As Figure 3 shows, we observe at least five refracted phases for which an interpretation is made: P_2, P_3, P_3S, P_3R, and S_3. We name refracted phases by the letter P or S to refer to the mode of propagation and by a number to indicate the layer of our model in which the wave propagates with grazing incidence. In this nomenclature, all up or down ray paths in the crust before or after grazing incidence are assumed to be of the same mode of propagation as the grazing ray. A discussion of example seismograms illustrating these phases is presented in the Appendix.

Travel-Time Corrections

Since the experimental site has a bottom relief of about 0.7 km with the slopes for some of the topographic highs occasionally as great as 10°, it is necessary to correct the travel-time data for the bottom relief. The travel-time correction for bottom relief is the product of a correction coefficient ($\Delta t/\Delta h$) and the difference (Δh) between the depth at which the refracted ray enters the sea floor and the depth of the OBS. These topographic corrections retain the water layer and flatten the sea floor to a horizontal datum. When $\Delta t/\Delta h$ is correctly estimated [see Whitmarsh, 1975] and the refractor is dipping, the resulting travel times measure the apparent velocity of the refractor.

As an approximation of Δh, the difference between the depth of the OBS and the depth beneath the shot was used instead of the difference between the depth of the OBS and the depth at which the ray enters the sea floor. This is a necessary approximation since azimuths of shooting lines are not always equal to the azimuths from the shots to the receivers. Using the depth beneath the shot results in a maximum error in the topographic correction for arrivals with, for example, apparent velocities around 6 km/sec of about 0.04 sec when shooting over a bottom with a 10° slope. The standard error of the travel-time picks for P_3 arrivals usually vary between 0.02 to 0.05 sec. For arrivals with apparent velocities around 4 km/sec the maximum error in the topographic correction is 0.06 sec when shooting over a 10° slope. The standard error of the travel-time picks for P_2 arrivals is about 0.025 sec. Fortunately, several of the refraction profiles are over sea

floor with very little dip for ranges at which P_2 is observed.

For each refraction line, we varied $\Delta t/\Delta h$ until we found a value that minimize the root-mean-square (RMS) of the travel-time residuals for each group of arrivals that we interpret to have the same apparent velocity. We show in Figure 4 the effect on the RMS of the travel-time residuals and least-squares apparent velocity and time intercepts of P_3 arrivals when $\Delta t/\Delta h$ is varied. (In this paper, the RMS of the travel-time residuals is referred to as "RMS".) The examples in Figure 4 are representative of the variation with $\Delta t/\Delta h$ of these travel-time parameters for the remaining profiles. In Figure 4 the RMS either has a minimum value for $\Delta t/\Delta h$ (OBS 2, line 7), a minimum over some range of $\Delta t/\Delta h$ (OBS 1, line 4) or no distinct minimum with $\Delta t/\Delta h$ (OBS 2, line 8). Since the values of both the apparent velocity and time intercept were strongly dependent on the correction coefficient without decreasing the RMS for line 8 (Figure 4), we conclude that the apparent velocity and time intercept for line 8 are not adequately determined for P_3 arrivals.

We did not have adequate control on the thickness of sediments beneath our shooting tracks even though there are several sediment ponds in faulted depressions and on the back sides of tilted fault-blocks in the crestal mountains [Macdonald and Luyendyk, 1977]. Therefore, the effect of the sediments on the travel times is neglected. Inspection of records of the 3.5 kHz precision depth recorder shows that most of the shots were over bare rock or very thin sediment. Thus, sediment corrections are not important for most of the refraction lines. Line 1, however, was shot over a sediment pond that follows a valley. Apparent velocities of P_3 may be low for this line since the average sediment

thickness increases in this valley towards the north [Whitmarsh, 1978]. We were able, using a few assumptions, to correct for the sediment thickness beneath the OBS's (discussed later).

Correlation of Travel-Time Residuals with Bottom Relief

In general, we observe for profiles approximately perpendicular to the average trend of the local topography and adjacent rift valley (lines 6 and 7) that the minimum RMS for P_3 arrivals is at or near the maximum theoretical value for $\Delta t/\Delta h$. A maximum value of $\Delta t/\Delta h$ implies a correlation of the uncorrected travel-time residuals and the velocity contrast between the water and the refractor [Whitmarsh, 1975]. That is, rays from the main refractor travel essentially the same distance through the material between the refractor and the sea floor. Macdonald and Luyendyk [1977] observe that most of the large-scale (> 2 km wavelength) bottom relief in the rift mountains have a faulted origin, probably block faulting. Thus, a correlation between the uncorrected travel-time residuals of the main refractor and the bottom topography suggests that the block faulting may extend into the crust to the depth of the main refractor.

Whitmarsh [1975] reports for a refractor observed at the same ranges as P_3 that the value of $\Delta t/\Delta h$ has lower value ($\Delta t/\Delta h$ = 0.25 sec/km) for a refraction line shot parallel to the topographic trends than the value of $\Delta t/\Delta h$ (0.57 sec/km) for two refraction lines shot perpendicular to the topographic trends in the eastern crestal mountains at 37°N. He suggests that the larger value of $\Delta t/\Delta h$ for the lines perpendicular to the topographic trends is a result of the lines

crossing block-faulted terrain. Whitmarsh suggests, however, that the value of $\Delta t/\Delta h$, 0.57 sec/km, observed for the refractor implies that the refractor may be unfaulted.

Time-Distance Data

We observe impulsive or easily identifiable first arrivals using a maximum charge size of 2.95 kg of TNT at ranges as great as 16 to 26 km on the various shooting tracks. The ground-waves have a predominant frequency of 15 to 20 Hz; this allows easily identifiable first arrivals at ranges less than 10 km to be picked to within 0.025 sec. First arrivals at ranges greater than about 10 km are read to 0.05 sec or better. Arrivals from shots fired directly over the tops of mountains were emergent. We unfortunately underestimated the charge size needed for ranges approximately 25 km and greater, and these seismograms also show emergent first arrivals. Only impulsive or easily identified arrivals have been used in the analysis of the travel-time data. The density of shots was great enough so that unacceptable seismograms could be ignored without seriously degrading the data set. In Figure 5 we present the travel times of first arrivals recorded by OBS 1 and OBS 2 as a function of range. The arrivals are corrected for topography.

Apparent Velocities

We analyzed data from eight profiles shot radially from OBS's 1 and 2 (Figure 1) to determine the azimuthal dependence of the apparent

velocities. Shipboard difficulties delayed the deployment of OBS 1 until the end of the second shooting line, but OBS 2 recorded shots from all eight profiles. A summary of the least-squares apparent velocities, time intercepts, RMS and $\Delta t/\Delta h$ for these compressional phases is given in Table I. Errors with a 95% confidence interval were calculated following Steinhart and Meyer [1961]. These errors yield the goodness of fit to the plane-layer model and do not estimate the accuracy of determining the actual velocity.

We observe large variations in the apparent velocities of P_2 and P_3 arrivals. The apparent velocities of P_3 as observed from each shooting track and determined independently at each OBS are in close agreement with each other, increasing our confidence that the wide range of apparent velocity for the main refractor is real.

Velocities for the Upper Layer. The apparent velocities of P_2, as measured on the shooting lines, are difficult to determine. There is not a minimum RMS for two of the eight profiles recorded by both OBS's from which to estimate the apparent velocity. Apparent velocities measured from two other profiles are probably meaningless because their time intercepts were less than the theoretical intercept expected for a sea-bed refractor with the same apparent velocity as measured from the two profiles. The apparent velocities of acceptable measurements range from 4.31 to 4.79 km/sec (Table I). The time intercepts of these arrivals are not significantly different.

Velocities for the Main Refractor. The RMS of the travel-time residuals for P_3 arrivals range between 0.02 and 0.07 sec for the radial refraction lines (Table I). This scatter is on the order of the accuracy of the reading error and the topographic corrections of these arrivals. There is a suggestion that the scatter of the travel-time data are not independent. For example, in Figure 5 several of the time-distance plots (line 4, OBS 1; line 6, OBS 1; line 3, OBS 2) show a scatter of the travel-time residuals from the least-squares line with an apparent wavelength of about 4 km. These data are corrected for topography and comparison of the bathymetry with the travel-time data in Figure 5 does not show any obvious relationship. The apparent velocities are somewhat dependent on the cause of this scatter, presumably a result of not accounting for the offset distance of the ray-path and variation in structure beneath the shots and along the ray-path of the arrivals. It is difficult to estimate the actual effect of the scatter on the apparent velocities and if the value of the apparent velocities represent a reasonable average of the effects of the scatter.

In Figure 6 we plot the apparent velocities of the main refractor from the radial profiles as a function of the azimuth of the shooting tracks (open symbols are considered unreliable measurements as discussed earlier). If all of the unreliable measurements are thrown out, then there is about a 16% variation from 5.62 to 6.61 km/sec. The variation of the apparent velocities measured in this experiment is within the observations of apparent velocities at similar ranges (5.6 to 7.21 km/sec) by previous studies in the vicinity.

The apparent velocity of shear arrivals, S_3, could only be measured on two of the shooting lines where it was observed. Table II lists pertinent time and velocity data for the two measurements of S_3. We consider the measurements from line 7, OBS 1 as the only reliable measurement. The measurements from line 3, OBS 2 consists of 4 travel-time readings over 5.5 km; whereas, measurements from line 7, OBS 1 consisted of 7 readings over 18.7 km.

Crustal Model

It is difficult to estimate the actual velocity of the upper layer since there is no simple geological model to account for the observed differences of the apparent velocities. For the purposes of solving for the actual velocity of the main refractor we chose to use the average of the apparent velocities of the upper layer. This average is 4.41$\pm$.30 km/sec if the velocities are weighted by the reciprocal of their standard deviations, and realistically evaluating the uncertainties of the determination, simply about 4.5 km/sec.

To estimate the actual velocity of the main refractor we assume that the variation of the apparent velocities is controlled by structure, and for a first approximation, by a simple dipping layer. This assumption, of course, neglects the effects of lateral structural changes along the profiles. These are six radial profiles in the data set that can be combined to form three split profiles and solved for the velocity of the main refractor (Table I). The velocities determined in this way are 6.37, 6.15 and 6.29 km/sec, whose average is 6.27$\pm$.11 km/sec; this result is quite insensitive to our choice of the

velocity for the upper layer. The dips implied by the model are away from the median valley and are between 1.4° and 1.7°. Correcting for the sediment thickness beneath each OBS, the dipping layer model implies a thickness of the upper layer of 1.7 km beneath OBS 1 and 1.6 km beneath OBS 2. This difference in the thickness of the upper layer beneath the instruments is not significant considering the resolution of this technique.

If we assume that the main refractor parallels the sea floor relief, correction for the topography with $\Delta t/\Delta h$ near its maximum theoretical value ($\sim$ 0.65 sec/km) yields travel times that measure the velocity of the refractor instead of the apparent velocity. Within the errors of measuring the velocities of P_3, the velocities for lines 6 and 7, OBS 2 suggest that 6.3 km/sec is a reasonable value for the actual velocity of the main refractor. If, on the other hand, the average dip of the main refractor does not parallel the sea floor, these velocities suggest that the average dip of the main refractor is slightly greater than the average dip of the sea floor and that the actual velocity is between the apparent velocities for those lines.

Estimating the thickness of the 6.3 km/sec material in the crestal mountains requires several assumptions since we do not observe a refraction with a higher velocity near the end of the profile, i.e., beyond 25 km. Assuming a 6.5 km/sec layer beneath the 6.3 km/sec and a minimum crossover distance of 25 km with refractions from a 6.5 km/sec layer results in a thickness of about 1.3 km for the 6.3 km/sec layer. The actual thickness could, of course, be greater if the velocity between the 6.3 km/sec layer and mantle is higher than 6.5 km/sec.

Having as a first approximation a dipping model for the main refractor, we can test various dipping-layer models to determine if they are consistent with the variations in the observed apparent velocities of the other profiles. In Figure 6 superimposed on the data points is a curve showing the azimuthal dependence of apparent velocity caused by a plane refractor parallel to the local strike of rift valley and dipping at 2° to the west. It is clear that all of the reliable data does not satisfy the variation of apparent velocity with azimuth for this or any smaller dip. Thus, although a first approximation of the structure from split profiles suggests an increase in depth of the main refractor away from the rift valley, a simple dipping model over the entire area of the experiment does not satisfy the data.

In Figure 7 we plot the time intercepts of the main refractor and their regression errors as a function of the azimuth of the shooting track. These time intercepts are corrected for the sediments beneath the OBS's. With the exception of line 6, all of the time intercepts measured from OBS 1 and OBS 2 for each line are almost equal, suggesting that we properly corrected for the sediments beneath each instrument. Again, if the time intercepts are consistent with a dipping-layer model over the entire area of the experiment, the time intercepts of all the lines should be approximately equal (a difference of less than 0.01 sec). Although this is the case for almost all of the lines used to form the split profiles, lines 4 and 5 have significantly different intercepts.

Converted Shear Waves

A large and persistent phase that is observed on the horizontal traces of OBS 1 and OBS 2 has the appearance of being a shear arrival converted from the compressional P_3 phase. Examples of this phase, P_3S, are shown in Figures 8a, 8b, 8c and 8g. This phase arrives about 0.55 sec after the P_3 arrival on OBS 1 and about 0.3 sec after P_3 on OBS 2. It is not likely that this phase is an instrumental effect since its particle motion differs significantly from that of the P_3 arrival and is, in fact, the particle motion expected for a shear arrival. The time delay between this phase and the P_3 arrival is essentially constant over all ranges though different on both instruments so that it has the same apparent velocity as P_3. We showed earlier that the main refractor can have a significant lateral variation in depth so the constant time difference argues strongly that this phase is converted directly beneath the instruments and not elsewhere along the ray-path. There are several places where the conversion to the shear mode could occur. Because the time delay is so different on the two instruments the simplest interpretation is that the conversion occurs at the base of the sediments. Very slow shear velocities of sediments mean that rather substantial time differences can be explained by acceptably minor differences in sediment thickness beneath the two instruments. This interpretation is strengthened by the occasional observation of a similar phase following P_2 by the same time delay (e.g., P_2S in Figure 8e).

Another interpretation for P_3S is that the conversion to a shear mode may occur at the base of layer 2A (T.C.G. Francis, written commun-

ication, 1977]. Francis observes similar converted phases on OBS seismograms of earthquakes. The OBS's, however, were on bare rock. If true, this implies a low shear velocity for layer 2A.

With the assumption that the converted phase, P_3S, is converted at the rock-sediment boundary, we can estimate the average shear velocity of the sediments. This assumption also suggests that the sediment thickness beneath OBS 2 is about 0.6 of that beneath OBS 1. A compressional velocity of 1.59 km/sec was measured for sediments (nanno-ooze) recovered from nearby DSDP hole 332B (unpublished report). The maximum sediment thickness in the neighborhood of the instruments determined by a two-way reflection time of 0.3 sec is about 0.24 km [Laughton, unpublished manuscript]. Assuming that this maximum thickness accounts for the greater time delay (on OBS 1), the maximum shear velocity of the sediments is then 0.34 km/sec. This implies a minimum Poisson's ratio of $\sigma = 0.48$. Similar values are measured in marine sediments elsewhere by ocean bottom instruments. Sutton et al. [1971] report shear velocities of the sediments ranging from 0.4 to 0.6 km/sec ($\sigma = 0.48$) beneath the Columbia University ocean bottom observatory off the California coast. Davis et al. [1976] find shear velocities in turbidites on the Juan de Fuca rise between 0.51 and 0.55 km/sec ($\sigma = 0.45$ to 0.455). The low shear velocities determined in this study are also consistent with shear velocities of deep-sea sediments measured from surface wave data. Sykes and Oliver [1964] calculate shear velocities between 0.2 and 0.4 km/sec for the upper 0.5 km of the Argentine Basin.

DISCUSSION

Crustal Structure at 37°N

The results of this OBS refraction experiment define a layer with an average velocity of 4.5 km/sec above a main refractor with a compressional velocity of 6.3 km/sec. Observed apparent velocities of refractions from the main refractor from split profiles suggest an increase of depth away from the median valley that is approximated by a dip of about 1.5°. It is difficult to estimate the reliability of the value of the dip because we show that the assumption of dipping layers is only a rough approximation. Thus, we simply interpret the implied dip as an indication of a deepening of the velocity surface in the crestal mountains away from the median valley, neglecting details of structural relief.

The increase of water depth away from the median valley in the crestal mountains is mostly accounted for by outward-facing faults and by some tilting of crustal blocks [Macdonald and Luyendyk, 1977]. Since our study of the travel-time residuals from refraction lines perpendicular to the median valley suggests that block-faulted structure exists at least down to the depth of 6.3 km/sec material, the increase of the depth of velocity surfaces in the crestal mountains in the direction away from the median valley may be controlled largely by the faulted structure.

The seismic data for both the upper layer and the main refractor do not suggest any sytematic cause for the azimuthal variation of apparent velocities. Faulted crustal blocks that flank the ridge axis

in the crestal mountains are observed with their tops dipping away from the ridge axis on the average of 3° to 4° [Macdonald and Luyendyk, 1977]. The scale of the experiment is too large, up to 35 km. to be confined to one faulted-block since the topography is characterized on a large scale by rolling relief of 6 to 12 km wavelength [Macdonald and Luyendyk, 1977]. It is conceivable that the measured dip of the main refractor represents an average of several faulted-blocks. Across the site of the experiment, magnetic lineations, between anomalies 2' and 3', change their trend from 17° to 40°, suggesting that accretion was not at a constant spreading rate and direction (see the paper by Macdonald [1977]). Thus, changing local conditions of crustal formation, may add further complications in determining crustal structure in the crestal mountains.

Main Refractor. We do not classify the main refractor in terms of average models presented by others for the oceanic crust since we do not observe a refractor of a higher velocity at depths below the main refractor. Furthermore, Orcutt et al. [1976] suggest, for crust less than 5 m.y. near the East Pacific Rise, that there is no clear stratification of velocities with depth typical of the distinct layering found in older oceanic crust. More detailed studies of crustal structure as a function of age are needed near the mid-Atlantic ridge before it is clear how young oceanic crust evolves into older oceanic crust.

Proposed Structure Section at 37°N. In the following discussion we compare our results with other refraction experiments at 37°N. We present and discuss the implications of a model of the upper crust at

37°N that is based on data from the better constrained refraction experiments at 37°N. We emphasize that our model is crude and that detailed experiments using reversed travel-time data and amplitude data to bottom instruments should yield more accurate models of the crust near the ridge crest.

The 6.3 km/sec main refractor observed in the crestal mountains by this study is low compared to velocities of refractors observed at the same ranges in the crestal mountains by Poehls [1974], Fowler and Matthews [1974] and Fowler [1976]. The data of Fowler and Matthews and Fowler were from unreversed profiles perpendicular to the structural trends and over the transition of the median valley into the crestal mountains. Fowler mentions that results from the lines should be treated with caution since lateral structural changes must be present. Poehls interpreted profiles essentially parallel to the structural trends in the crestal mountains. Although Poehls treated two profiles as reversed-profiles, time-distance plots of these profiles indicate that reciprocity of travel-times between the shots and receivers, required by a reversed profile, is not satisfied. Data from these two profiles were interpreted without topographic corrections; this would have a large effect, as shown in this paper, on the measured apparent velocities when shooting over rough topography.

Whitmarsh [1978] presents velocity-depth models from a refraction line (profile 8443) shot to a bottom hydrophone and parallel to the structural trends in the crestal mountains. The refraction line is approximately 2 km east of and parallel to line 1. In Figure 9 we compare his gradient model with the two-layer model determined from this study. The agreement between these models in the upper 1.5 km

is not good. This is not surprising since we assume one layer and have less travel-time data for the upper crust than Whitmarsh. (His shot spacing was about 0.25 km). Both models, however, reach velocities of 6.3 km/sec at similar depths (about 1.6 km for this study and about 1.8 km for Whitmarsh). The depth of the 6.3 km/sec velocity is shallower for our model than for the model of Whitmarsh. This is expected since thick-layered models yield estimates of depth for a given velocity that are smaller than estimated from gradient models [Kennett and Orcutt, 1976].

A velocity-depth model for the East Pacific Rise (EPR) determined by Orcutt et al. [1976] for crust of the same age as the crust studied by us is also shown in Figure 9. (The model of Orcutt et al. uses many thin layers to approximate a gradient with depth.) Again, there are large differences between the velocity model of the EPR and the mid-Atlantic ridge in the upper 2 km of the crust. But it is striking that below 2 km the velocities of all of these models are similar. The spreading rate (half-rate) of the EPR near the refraction experiment is about 6 cm/yr [Orcutt et al., 1976] and the spreading rate at 37°N is about 1 cm/yr [Macdonald, 1977]. The similarity of velocity structure at depth for the models in Figure 9 may not be surprising if the gross velocity structure observed in oceanic crust is controlled mainly by petrological processes that are relatively independent of spreading rate.

Fowler [1976] presents a detailed velocity-depth model of the crust beneath the median valley from a refraction line centered over the inner floor of the median valley. The model of Fowler is constrained by travel-time and amplitude data and uses several layers to approxi-

mate a velocity transition with depth.

In Figure 10 we propose a structure section of the mid-Atlantic ridge at 37°N based on the results of Fowler [1976] at the median valley and the results of this study and the study of Whitmarsh [1978] in the crestal mountains. The structure shown in Figure 10 beneath the crestal mountains represents a summary of both studies. We do not mean to imply that the actual structure beneath the crestal mountains is as simple as portrayed.

Large temperature variations are expected in the crust near a spreading center and any comparison of crustal models in Figure 10 has to account for the temperature effects on the velocities. Murase and McBirney [1973] report the effect of temperature on the seismic velocities (at atmospheric pressures) of a tholeiitic basalt. They show that the compressional velocity of the basalt varies only a little below 800°C but that the velocity rapidly decreases at higher temperatures until the melting temperature is reached. A thermal model for the oceanic crust at 37°N by Sleep [1975] predicts that temperatures for the upper 2 km do not exceed 800°C except within a kilometer of the ridge axis. The decrease of temperature in the crust predicted away from the vicinity of the ridge axis by Sleep is several hundred degrees. Thus, the temperature coefficient for velocity of gabbroic rock [Birch, 1958] and the results of Murase and McBirney suggest that the seismic velocities of the upper crust may increase 0.2 to 0.3 km/sec away from the axis. Hydrothermal circulation at the ridge crest, if it exists, would cause a more rapid loss of heat than predicted by the model of Sleep and lower temperatures in the crust [Sleep, 1975]. Shear waves are observed propagating across the axis

at 37°N and preclude the existence of any sizeable magma chamber at shallow depth [Fowler, 1976] that makes a comparison between the velocity models more uncertain.

The depth to velocities of 6.3 km/sec beneath the bottom instruments in the crestal mountains, about 1.6 to 1.8 km, is relatively well constrained. The depth of the 6.3 km/sec material beneath the crestal mountains and the velocity structure near the center of the median valley suggest a difference of depth exists between material beneath these two areas (Figure 10). Thus, any value of dip for the main refractor away from the median valley in Figure 10, even zero dip, implies a lateral change in velocity structure from the median valley to the crestal mountains. The structural model suggests that the greatest lateral change in velocity structure occurs within the median valley. That is, the boundary of the outer wall of the median valley with the crestal mountains apparently marks the point where the maximum difference in depth occurs between material of a similar velocity ($\sim$ 6.2 km/sec). This difference in depth (for reasonable values of dip of the $\sim$ 6.2 km/sec refractor) is approximately 1.5 km and is almost the same as the topographic relief of the median valley. These observations suggest that processes that cause the topographic relief of the median valley are deeper than 2 or 3 km in the crust.

The model in Figure 10 also suggests that material of a similar velocity (about 6.2 to 6.3 km/sec) occurs at approximately the same depth beneath the sea floor beneath both the inner floor of the median valley and the crestal mountains. This result is independent of the implied dip in Figure 10 of the 6.3 km/sec material in the crestal mountains. A constant depth beneath the sea floor is easily

maintained by a block-faulted structure. Atwater and Mundie [1973] and Macdonald and Luyendyk [1977] suggest that the topographic relief of median valleys is accounted almost entirely by block faulting. Both the existence of relief between material at depth and the constant crustal thickness above the 6.2 to 6.3 km/sec material supports the hypothesis of Atwater and Mundie and of Macdonald and Luyendyk. Thus, processes such as off-axis intrusion causing a thickening of material for the upper 2 to 3 km are not necessary. Off-axis intrusion may, however, be important for material at greater depth. The hypothesis of block faulting and the structural section are also consistent with depths of 3±2 km suggested by Weidner and Aki [1973] for earthquakes characterized by normal-faulting at the ridge crest.

One consequence of the constant thickness for the upper portion of the crust beneath the crestal mountains and inner floor of the median valley is that most of the upper 2 km of crust is probably formed near the inner floor of the median valley. This aspect of the proposed structural section is consistent with the inference from magnetic studies at 37°N [Macdonald, 1977] that a narrow zone of intrusion (2 to 3 km wide) and that over 90% of extrusive volcanism occur within the inner floor of rift valley 2.

Variation of Travel-Times Across Fracture Zone A

Refraction line 1 was extended to cross fracture zone A, which offsets the rift valley about 20 km [Arcyana, 1975]. The purpose was to evaluate in a simple manner the effect, if any, upon the travel-times of seismic waves transmitted through crust which is in part a product of

transform domain tectonics. Numerous fault scarps are observed farther to the east of line 1 in the axis of transform A [Detrick et al., 1973; Arcyana, 1975]. Also mafic and ultramafic rocks are typically recovered from transform fault terrain and many of these rocks exhibit cataclastic textures [e.g., Bonatti and Honnorez, 1976; Fox et al., 1976]. It was therefore anticipated that the travel-times of compressional waves propagating through the crust of fracture zone A would contrast with travel-times of normal oceanic crust.

The location of refraction line 1, OBS 2 and fracture zone A are shown in Figure 11. In the vicinity of our experiment fracture zone A trends roughly east-west near latitude 37°02'N [V. Renard, personal communication, 1976], and is about 10 km wide with a floor about 200 m deeper than the sea floor to the south. A seismic reflection profile conducted within 1 km of line 1 by the VEMA (V32-03) shows less than 0.2 sec of sediments in the trough of the fracture zone. Farther west two other VEMA reflection profiles, also showing a sediment-filled trough, suggest that in terms of basement relief the fracture zone can still be traced as far as 33°40'W (Figure 11).

Along line 1, from north to south, the topography of the fracture zone (Figure 12) is characterized by an apparently rough bottom with little sediments (beneath shots 42 to 37), giving way to smooth, sediment-covered bottom (beneath shots 37 to 29). The southern boundary of the fracture zone is not apparent from the topography.

In Figure 12 the negative travel-time residuals (early arrivals) for shots 27 to 38 over the fracture zone show that compressional waves arrive earlier than they would if the crust of the fracture zone had the same velocity structure as the crust to the south of shot 26. There-

fore, a higher compressional velocity is implied for the crust of the fracture zone by these travel-times. Although the shot size was adequate along other profiles at similar ranges, ground-wave arrivals from shots 39 to 43 were very emergent and could not be picked reliably. The increase of scatter in the travel-time residuals occurs in only a kilometer (shots 26 to 28), indicating substantial lateral heterogeneity in the crust and possibly the southern boundary of the fracture zone.

We suggest that intrusives are primarily responsible for the relatively higher velocity within the fracture zone. Since at present there is little evidence that crust formed near transform/rift valley junctions differs significantly in composition from crust formed at the rift valley, we would not expect higher velocities for crust in the fracture zone. One would expect, however, lower velocities since transform tectonics (faulting, brecciation), when compared to "normal" oceanic crust accreted at the rift valley, are likely to lower the average velocity of the country rock. The observed higher velocity suggests the introduction of rock not significantly altered by faulting or different from normal oceanic crust. The abrupt change of travel-time residuals over a short distance supports this interpretation.

Other evidence has been presented for accretion along fracture zones. Dolerite intrusives associated with faults have been sampled east of line 1 on the northern scarps of transform A [Arcyana, 1975]. Cochran [1973], on the basis of magnetic and gravity data, suggests that large fracture zones serve as the site of intrusion of large quantities of ultramafic rocks from depth. Along other fracture zones elongate ridges are oriented parallel to the strike of transform faults

[Heezen et al., 1964a; Heezen et al., 1964b; Van Andel et al., 1967; Johnson, 1967; Fleming et al., 1970; Thompson and Melson, 1972]. These ridges are interpreted by Bonatti [1973] as fault-bounded blocks of partially serpentinized ultramafic rock. Fox et al. [1976] suggest that these elongate ridges are likely topographic expressions of either diapiric intrusions of partially hydrated upper mantle or the intrusion and extrusion of basaltic magmas.

Coarse-grained intrusives have been drilled from shallow depths below the acoustic basement near 37°N. At DSDP site 334, located west of line 1 approximately along the projected east-west strike of fracture zone A, Melson et al. [1974] describe a gabbro and partially serpentinized peridotite complex at shallow depths underlying extrusive basalts. Compressional velocities of these gabbros and peridotites are considerably higher than those of the basalts (average 5.95 km/sec at 0.5 Kbar), which are thought to comprise most of the upper crust. Velocities of the recovered gabbros and peridotites range between 6.5 to 7.29 km/sec at 0.5 Kbar [Melson et al., 1974]. The shallow emplacement of these coarse-grained intrusives at site 334 raises the possibility of similar occurrences of shallow intrusives lying along the axis of fracture zone A.

CONCLUSIONS

1. Observations of a converted shear wave, P_3S, presumably converted at the rock-sediment interface beneath the OBS's suggest that the average shear velocity of sediments beneath the OBS's is no greater than 0.34 km/sec.

2. The velocities of material above the main refractor are poorly constrained by our refraction experiment. The average of apparent velocities observed from several of the radial profiles is about 4.5 km/sec.

3. A main refractor with a velocity of 6.3 km/sec occurs about 1.7 km beneath the OBS's in the crestal mountains. Apparent velocities of the main refractor from split profiles suggest that the depth of the main refractor increases away from the median valley.

4. Values of the topographic correction factor, $\Delta t/\Delta h$, observed for the main refractor from lines perpendicular to topographic trends suggest that block-faulted structure may extend to the depth of the main refractor.

5. Several observations are made from a proposed structural section for the upper crust at the mid-Atlantic ridge. The structural section is based on results from the better constrained refraction experiments at 37°N. There is a difference in depth between material of similar velocity at a depth of about 1.7 to 2.0 km beneath the inner floor of the median valley and beneath the OBS's in the crestal mountains. This difference increases over a distance of 10 to 15 km away from the inner floor and decays in the crestal mountains. The maximum amount of relief, about 1.5 km, is the same as the topographic relief for the median valley and probably occurs at the boundary of the median valley with the crestal mountains. Material with a velocity of around 6.2 to 6.3 km/sec is approximately at similar depths beneath the sea floor in both the crestal mountains and the median valley. A narrow zone of intrusion, probably within the inner floor, for

the upper 2 km of crust is suggested by the structural section.

6. Large, travel-time residuals, averaging -0.2 sec, observed from a refraction line over fracture zone A indicate that portions of the crust of the fracture zone may have higher average velocities than oceanic crust outside of the fracture zone. It appears that strong heterogeneity of the crust exists over a few kilometers near the boundary of the fracture zone.

ACKNOWLEDGEMENTS

We would like to thank H. Kohler and the officers and crew of the R/V VEMA for their valuable assistance. Special thanks go to W. McDonald, R. Bookbinder, G. Gunther and A. Hubbard for their work with the ocean bottom seismographs in the field. V. Renard was kind enough to let us use a bathymetric chart that he compiled. M. Purdy made many helpful suggestions for improving the manuscript. We thank J. Ewing, L. R. Sykes, and A. B. Watts for critically reviewing the manuscript. This study was supported by the National Science Foundation under grant NSF DES74-24698 and Office of Naval Research grant N00014-76-C-0818.

REFERENCES

Arcyana, Transform fault and rift valley from bathyscaph and diving saucer, Science, 190, 108-116, 1975.

Atwater, T., and J.D. Mudie, Detailed near-bottom geophysical study of the Gorda Rise, J. Geophys. Res., 78, 8665-8686, 1973.

Birch, F., Interpretation of the seismic structure of the crust in light of experimental studies of wave velocities in rocks, Contributions to Geophysics in Honour of Beno Gutenberg, Pergamon Press: New York, pp. 158-170, 1958.

Bonatti, E., Origin of offsets of the mid-Atlantic ridge in fracture zones, J. Geol., 81, 144-165, 1973.

Bonatti, E., and J. Honnorez, Sections of the Earth's crust in the Equatorial Atlantic, J. Geophys. Res., 81, 4104-4116, 1976.

Cochran, J.R., Gravity and magnetic investigations in the Guiana Basin, western equatorial Atlantic, Geol. Soc. Amer. Bull., 84, 3249-3268, 1973.

Davis, E.E., C.R.B. Lister, and B.T.R. Lewis, Seismic structure of the Juan de Fuca Ridge: ocean bottom seismometer results from the median valley, J. Geophys. Res., 81, 3541-3555, 1976.

Detrick, R.S., J.D. Mundie, B.P. Luyendyk, and K.C. Macdonald, Near-bottom observations of an active transform fault (mid-Atlantic ridge at 37°N), Nature Phys. Sci., 246, 59-61, 1973.

Fleming, M.S., N.Z. Cherkis, and J.R. Heirtzler, The Gibbs fracture zone: a double fracture zone at 52°30'N in the Atlantic Ocean, Mar. Geophys. Res., 1, 37-45, 1970.

Fowler, C.M.R., Crustal structure of the mid-Atlantic ridge crest at 37°N, Geophys. J. R. astr. Soc., 47, 459-491, 1976.

Fowler, C.M.R., and D.H. Matthews, Seismic refraction experiment on the mid-Atlantic ridge in the Famous area, Nature, 249, 752-754, 1974.

Fox, P.J., E. Schreiber, H. Rowlett, and K. McCamy, The geology of the Oceanographer fracture zone: a model for fracture zones, J. Geophys. Res., 81, 4117-4128, 1976.

Heezen, B.C., E.T. Bunce, J.B. Hersey, and M. Tharp, Chain and Romanche fracture zones, Deep Sea Res., 11, 11-13, 1964a.

Heezen, B.C., R.D. Gerard, and M. Tharp, The Vema fracture zone in the equatorial Atlantic, J. Geophys. Res., 69, 733-739, 1964b.

Helmberger, D.V., and G. B. Morris, A travel time and amplitude interpretation of a marine refraction profile: primary waves, J. Geophys. Res., 74, 483-494, 1969.

Houtz, R., and J. Ewing, Upper crustal structure as a function of plate age, J. Geophys. Res., 81, 2490-2498, 1976.

Johnson, G.L., North Atlantic fracture zone near 53°N, Earth Planet. Sci. Lett., 2, 445-448, 1967.

Keen, C.E., and C. Tramontini, A seismic refraction survey on the mid-Atlantic ridge, Geophys. J. R. astr. Soc., 20, 473-491, 1970.

Kennett, B.L.N., and J.A. Orcutt, A comparison of travel time inversions for marine refraction profiles, J. Geophys. Res., 81, 4061-4070, 1976.

LePichon, X., R.E. Houtz, C.L. Drake, and J.E. Nafe, Crustal structure of the mid-ocean ridges, 1. Seismic refraction measurements, J. Geophys. Res., 70, 319-339, 1965.

Macdonald, K.C., Near-bottom magnetic anomalies, asymmetric spreading, oblique spreading, and tectonics of the accreting plate boundary on the mid-Atlantic ridge near 37°N, Geol. Soc. Amer. Bull., 88, 541-555, 1977.

Macdonald, K.C., and B.P. Luyendyk, Deep-tow studies of the structure of the mid-Atlantic ridge crest near lat. 37°N, Geol. Soc. Amer. Bull., 88, 621-636, 1977.

McDonald, W.G., A.C. Hubbard, R.G. Bookbinder, and K. McCamy, Design and shipboard operation of a multipurpose ocean bottom seismograph, Mar. Geophys. Researches, 3, 179-196, 1977.

Melson, W., and others, Leg 37 — the volcanic layer, Geotimes, 19, 16-18, 1974.

Murase, T., and A.R. McBirney, Properties of some common igneous rocks and their melts at high temperatures, Geol. Soc. Am. Bull., 84, 3563-3592, 1973.

Orcutt, J.A., B.L.N. Kennett, and L.M. Dorman, Structure of the East Pacific Rise from an ocean bottom seismometer survey, Geophys. J.R. astr. Soc., 45, 305-320, 1976.

Poehls, K.A., Seismic refraction on the mid-Atlantic ridge at 37°N, J. Geophys. Res., 79, 3370-3373, 1974.

Raitt, R.W., The crustal rocks, in The Sea, vol. 3, M.N. Hill, ed., pp. 85-102, Wiley, New York, 1963.

Shor, G.G., Jr., H.W. Menard, and R.W. Raitt, Structure of the Pacific Basin, in The Sea, vol. 4, part 2, A.E. Maxwell, ed., Wiley, New York, pp. 3-27, 1970.

Sleep, N.H., Formation of oceanic crust: some thermal constraints, J. Geophys. Res., 80, 4037-4042, 1975.

Steinhart, J.S., and R.P. Meyer, Explosion studies of continental structure, Carnegie Inst. Wash. Publ. 622, 409 pp., 1961.

Sutton, G.H., G.C. Maynard, and D.M. Hussong, Widespread occurrence of a high-velocity basal layer in the Pacific crust found with repetitive sources and sonobuoys, in The Structure and Physical Properties of the Earth's Crust, Geophys. Monogr. Ser., vol. 14, J.G. Heacock, ed., pp. 193-209, AGU, Washington, 1971.

Sykes, L. R., and J. Oliver, The propagation of short-period seismic surface waves across oceanic areas, Part II — analysis of seismograms, Bull. Seism. Soc. Amer., 54, 1373-1415, 1964.

Talwani, M., C.C. Windisch, and M.G. Langseth, Reykjanes Ridge crest: a detailed geophysical study, J. Geophys. Res., 76, 473-517, 1971.

Thompson, G., and W.G. Melson, The petrology of oceanic crust across fracture zones in the Atlantic Ocean: evidence of a new kind of sea floor spreading, J. Geol., 80, 526-538, 1972.

Van Andel, T.H., J.B. Corliss, and V.T. Bowen, The intersection between the mid-Atlantic ridge and the Vema fracture zone in the North Atlantic, J. Mar. Res., 25, 343-351, 1967.

Weidner, D.J., and K. Aki, Focal depth and mechanism of mid-ocean ridge earthquakes, J. Geophys. Res., 78, 1818-1831, 1973.

Whitmarsh, R.B., Median valley refraction line, mid-Atlantic ridge at 37°N, Nature, 246, 297-299, 1973.

Whitmarsh, R.B., Axial intrusion zone beneath the median valley of the mid-Atlantic ridge at 37°N detected by explosion seismology, Geophys. J. R. astr. Soc., 42, 189-215, 1975.

Whitmarsh, R.B., Seismic studies of the upper igneous crust in the North Atlantic and porosity estimates for layer 2, Earth Planet. Sci. Lett., 37, 451-464, 1978.

TABLE 1 — COMPRESSIONAL ARRIVALS

		P_3 Arrivals				P_2 Arrivals			
OBS	Line	Velocity (km/sec)	Intercept (sec)	Δt/Δh (sec/km)	RMS (sec)	Velocity (km/sec)	Intercept (sec)	Δt/Δh (sec/km)	RMS (sec)
1	3	6.19±.37	1.70±.11	.28	0.067	--------	--------	---	-----
1	4	6.60±.17	1.79±.06	.47	0.049	4.13±.74	1.24±.16	.47	0.025
1	5	5.62±.24	1.58±.07	.56	0.049	--------	--------	---	-----
1	6†	6.57±.19	1.77±.06	.56	0.038	--------	--------	---	-----
1	7†	6.19±.13	1.71±.06	.65	0.051	--------	--------	---	-----
2	1**	5.65±.20	1.65±.06	.36	0.025	--------	--------	---	-----
2	2†	6.01±.20	1.62±.08	.56	0.066	--------	--------	---	-----
2	3†	6.30±.32	1.63±.09	.56	0.050	4.72±.54	1.26±.09	.32	0.028
2	4	6.61±.15	1.74±.04	.57	0.033	4.24±.46	1.21±.09	.56	0.027
2	5	5.66±.33	1.54±.10	.47	0.055	--------	--------	---	-----
2	6†	6.44±.21	1.65±.06	.65	0.033	--------	--------	---	-----
2	7†	6.15±.24	1.65±.08	.65	0.047	--------	--------	---	-----
2	8*	6.80±.51	1.69±.11	.52	0.022	4.79±.1.12	1.26±.19	.36	0.027

† lines used to form split profiles.

* poorly determined with forced topographic correction.

** low velocity, sediment correction needed.

TABLE II — SHEAR ARRIVALS

OBS	Line	Velocity (km/sec)	Intercept (sec)	Δt/Δh (sec/km)	RMS (sec)	n
1	7	3.46±.14	2.61±.24	.57	0.066	7
2	3	3.23±.15†	1.97±.18†	.28	0.014	4

† unreliable, too few data.

FIGURE CAPTIONS

Figure 1: Location of the seismic refraction experiment with respect to the median valley and DSDP holes 332 and 333 (solid triangles). OBS's (solid circles) are identified by the thick, bold numbers. Thick, dark lines represent the shooting track. Shooting track with circled numbers represent the eight radial profiles discussed in this paper. Bathymetry is in uncorrected fathoms.

Figure 2: Record section of seismograms for line 4 recorded by the hydrophone channel of OBS 1. Bathymetry beneath line 4 is plotted below the record section. See text for details.

Figure 3: Schematic ray-path diagram (above) and time-distance plot (below) of seismic phases observed during this experiment. Explanations of the refracted phases are in the text. P_3 is the most prominantly observed arrival. The ray-path for P_3S is not shown.

Figure 4: Plots of RMS and least-squares velocities (V_N) and intercepts (To) as a function of $\Delta t/\Delta h$ for P_3 arrivals. Arrow denotes value of $\Delta t/\Delta h$ with a minimum RMS.

Figure 5: Time-distance data of the radial shooting lines recorded by OBS 1 and OBS 2. Travel-times are reduced by a velocity of 6 km/sec (T_R). Least-squares lines are drawn through P_2 and P_3 arrivals (solid circles). Crosses represent arrivals not used in least-squares solutions. The apparent velocities are given next to least-squares lines. Bathymetry beneath the shooting track is plotted below each time-distance plot at a vertical exaggeration of $\sim$ 4.

Figure 6: Apparent velocities and their 95% regression errors for refractions from the main refractor measured at OBS 1 (circles) and at OBS 2 (squares) plotted as a function of the azimuth of the shooting lines. Closed symbols represent reliable measurements; open are suspect measurements. The numbers denote line number. The curved line is the theoretical value of apparent velocities as a function of azimuth, assuming a true velocity of 6.3 km/sec, for a plane refractor dipping at an angle of 2° away from and striking parallel to the trend of the adjacent median valley. The data show that a simple, dipping refractor does not occur at the area of the entire experiment.

Figure 7: Time intercepts and their regression errors for refractions from the main refractor measured at OBS 1 (circles) and OBS 2 (crosses) as a function of the azimuth of the shooting track.

Figure 8: Seismograms recorded by OBS 1 and OBS 2 during experiment. The horizontal (H), vertical (V) or hydrophone (HP) channel is shown. The geophone traces were filtered between 15 and 30 Hz. The hydrophone traces were band-pass filtered between 15 and 30 Hz or high-pass filtered over 50 Hz. Seismic phases (P_2, P_2S, P_3, P_3R and P_3S) are labeled and are discussed in the text. The phases W_1 and W_2 are the direct water wave and the first bounce mode. Ranges of shots recorded by seismograms a through g are: 8.5, 5.8, 8.8, 4.5, 3.4, 17.8 and 15.2 km, respectively.

Figure 9: Velocity-depth models of the crestal mountains at 37°N from this study and from Whitmarsh [1978]. The velocity-depth model of the East Pacific Rise north of the Siqueiros fracture zone is from Orcutt et al. [1976]. Depths are below the sea-bed.

Figure 10: Proposed structure section of the mid-Atlantic ridge at 37°N. The structure section is approximately perpendicular to the strike of the median valley (rift valley 2). Velocity-depth model beneath the center of the median valley is after Fowler [1976]. Velocity model below the western crestal mountains is based on this study and the study of Whitmarsh [1978]. Existing data are not adequate at this time to resolve the details of the change of structure from the median valley to the crestal moun-

tains (denoted by dashed lines with queries). See text for a discussion of the tectonic implications of the model.

Figure 11: Locations of OBS 2 (triangle), refraction line 1 (solid line) and VEMA (32-03) seismic refraction lines (dashed lines) near 37°N. Fracture zone A is delineated by the 1200 fathom contour until about 33°34'W. Farther west the fracture zone probably follows a sediment filled trough until about 33°40'W. Bathymetry (corrected fathoms) is taken from a chart by V. Renard [personal communication, 1976].

Figure 12: Travel-time residuals (observed-calculated) of first arrivals and bottom topography (uncorrected meters) as a function of shot number along the track of line 1. The calculated travel-time is the travel-time of the least-squares curve for P_3 arrivals along line 1 for shots 12 through 26.

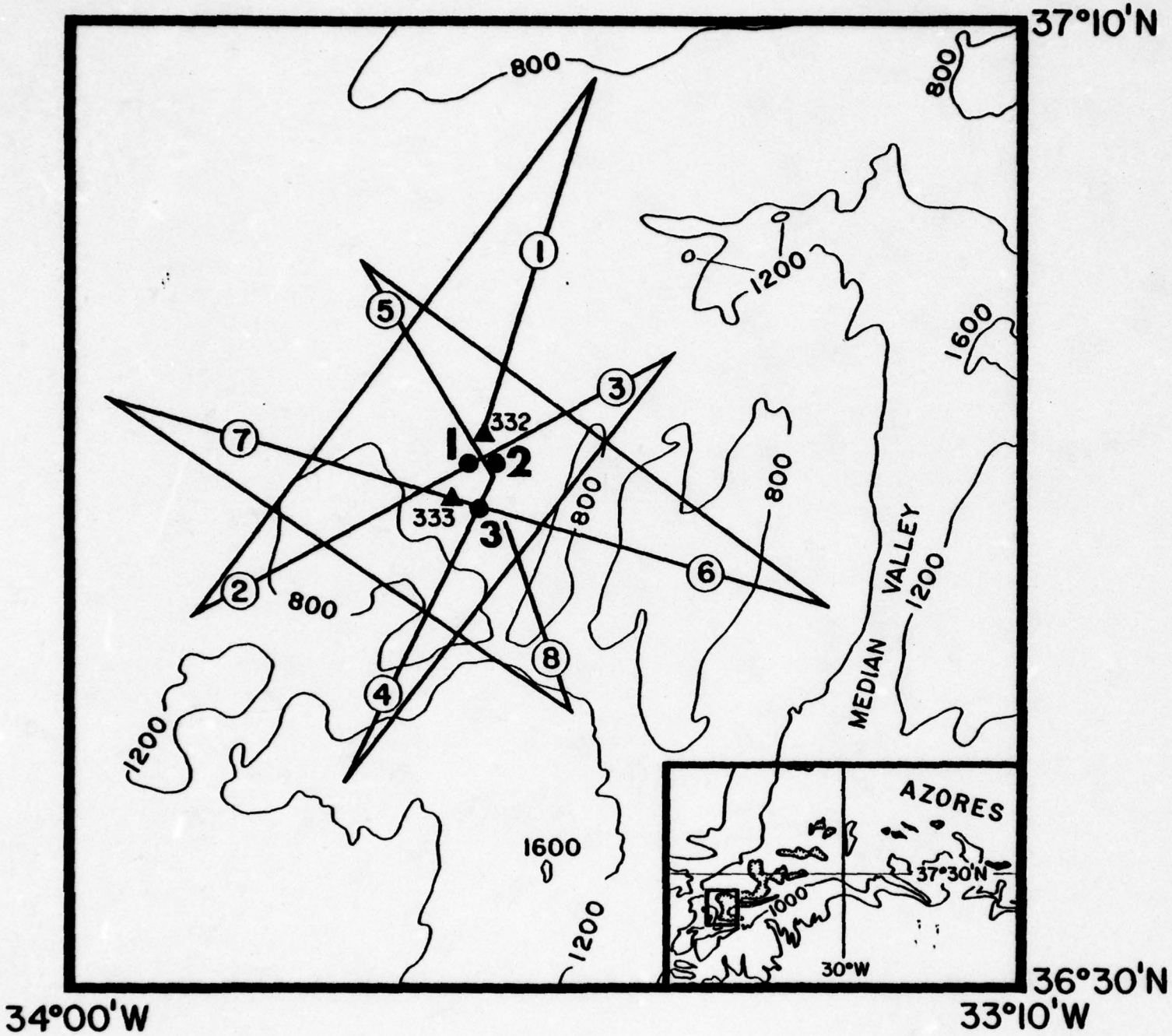
37°10'N
800
800
1200
1600
800
800
800
1200
MEDIAN VALLEY
1200
1600
1200
800
332
333
1
2
3
1
2
3
4
5
6
7
8
AZORES
37°30'N
1000
30°W
36°30'N
34°00'W
33°10'W

Figure 1

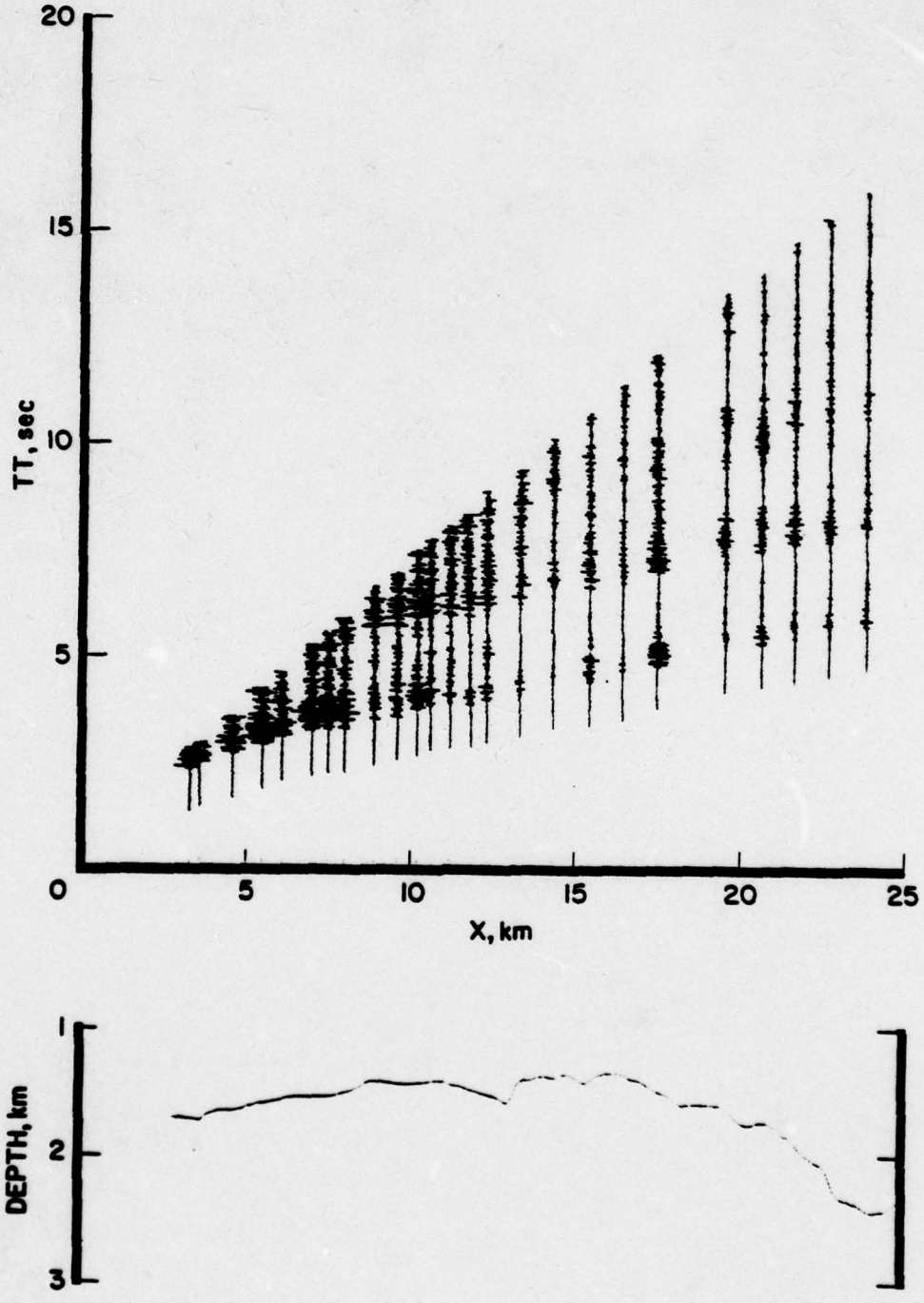

Figure 2

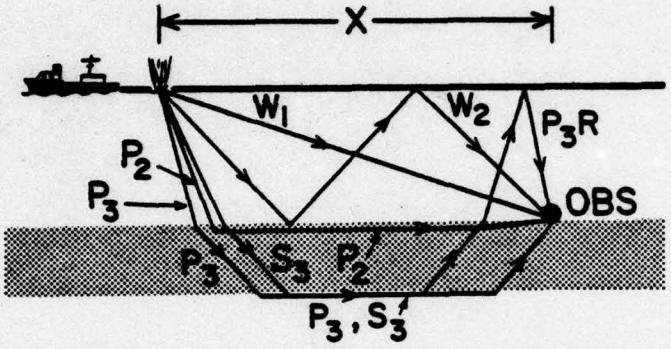
X
W1
W2
P3R
P2
P3
OBS
P3
S3
P2
P3, S3

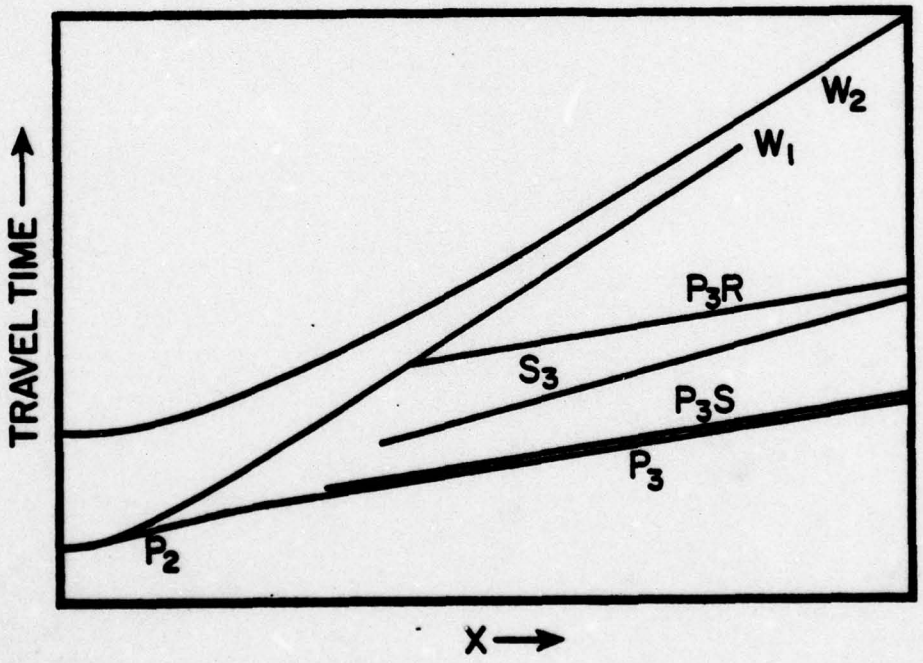
TRAVEL TIME
W2
W1
P3R
S3
P3S
P3
P2
X

Figure 3

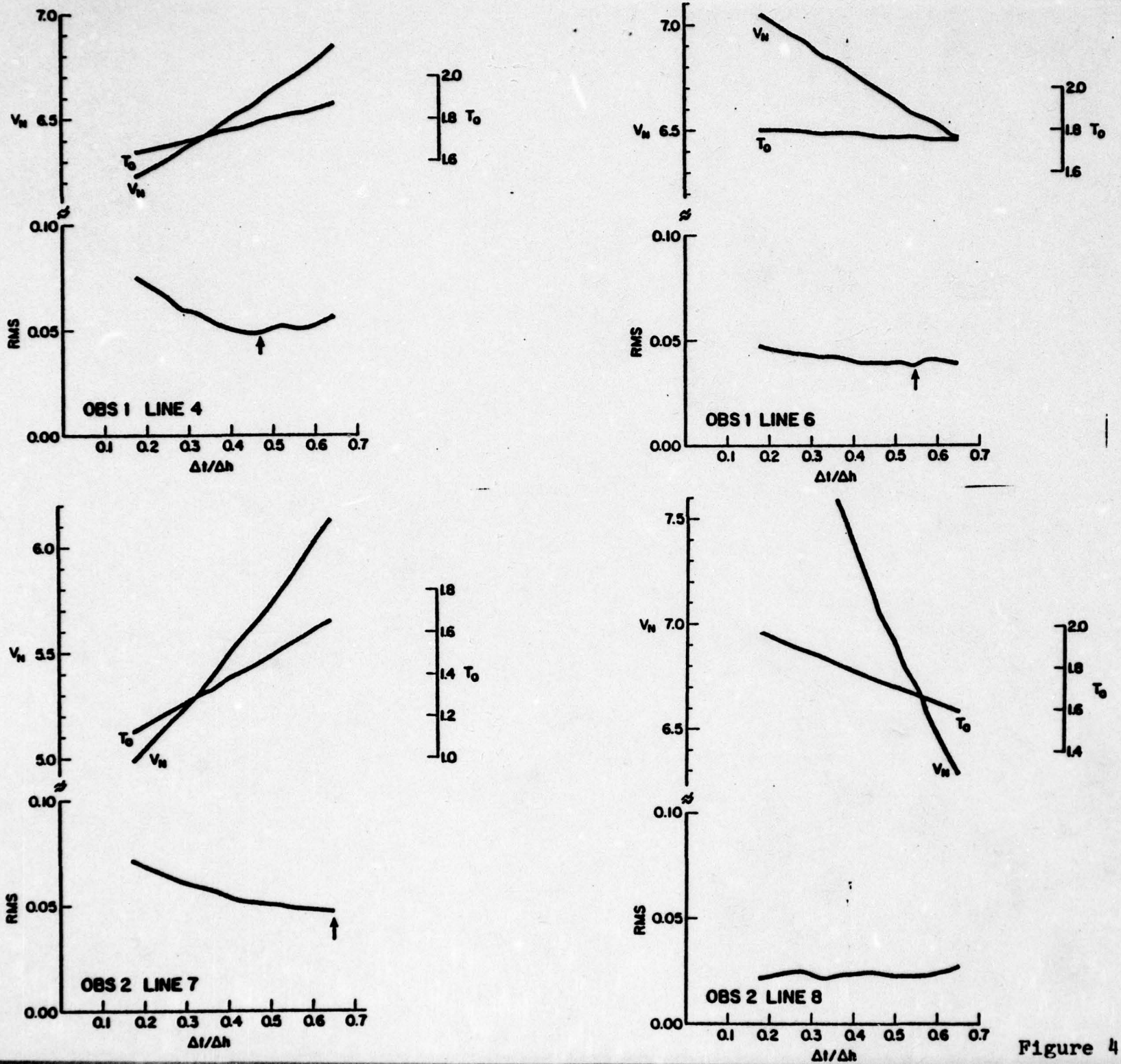
7.0
V_N 6.5
T_0
V_N
2.0
1.8 T_0
1.6
0.10
RMS 0.05
0.00
OBS 1 LINE 4
0.1 0.2 0.3 0.4 0.5 0.6 0.7
Δt/Δh
7.0
V_N
V_N 6.5
T_0
2.0
1.8 T_0
1.6
0.10
RMS 0.05
0.00
OBS 1 LINE 6
0.1 0.2 0.3 0.4 0.5 0.6 0.7
Δt/Δh
6.0
V_N 5.5
5.0
T_0
V_N
1.8
1.6
1.4 T_0
1.2
1.0
0.10
RMS 0.05
0.00
OBS 2 LINE 7
0.1 0.2 0.3 0.4 0.5 0.6 0.7
Δt/Δh
7.5
V_N 7.0
6.5
T_0
V_N
2.0
1.8
T_0
1.6
1.4
0.10
RMS 0.05
0.00
OBS 2 LINE 8
0.1 0.2 0.3 0.4 0.5 0.6 0.7
Δt/Δh

Figure 4

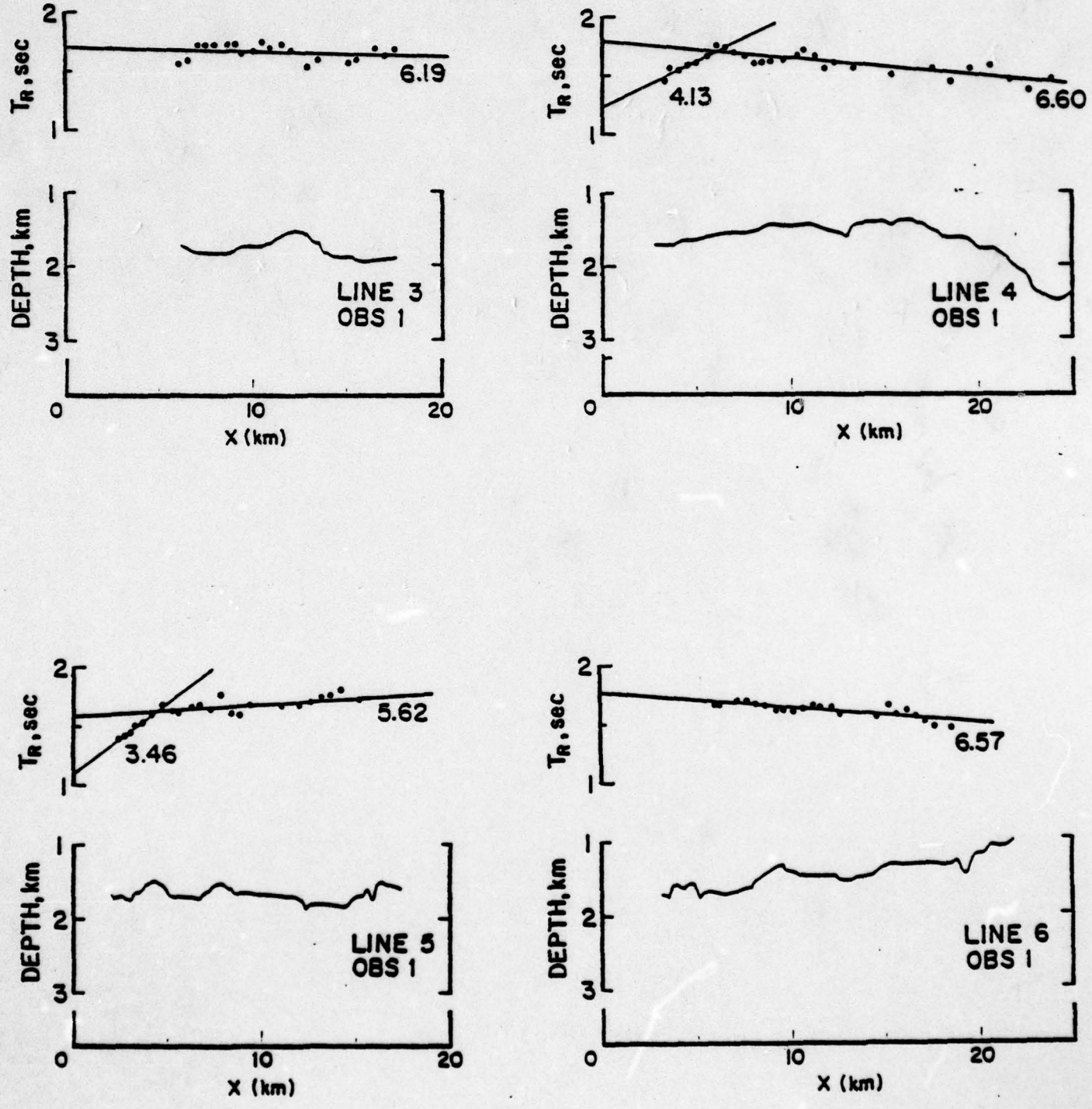
T_R, sec
6.19
DEPTH, km
LINE 3
OBS 1
X (km)
4.13
6.60
LINE 4
OBS 1
3.46
5.62
LINE 5
OBS 1
6.57
LINE 6
OBS 1

Figure 5

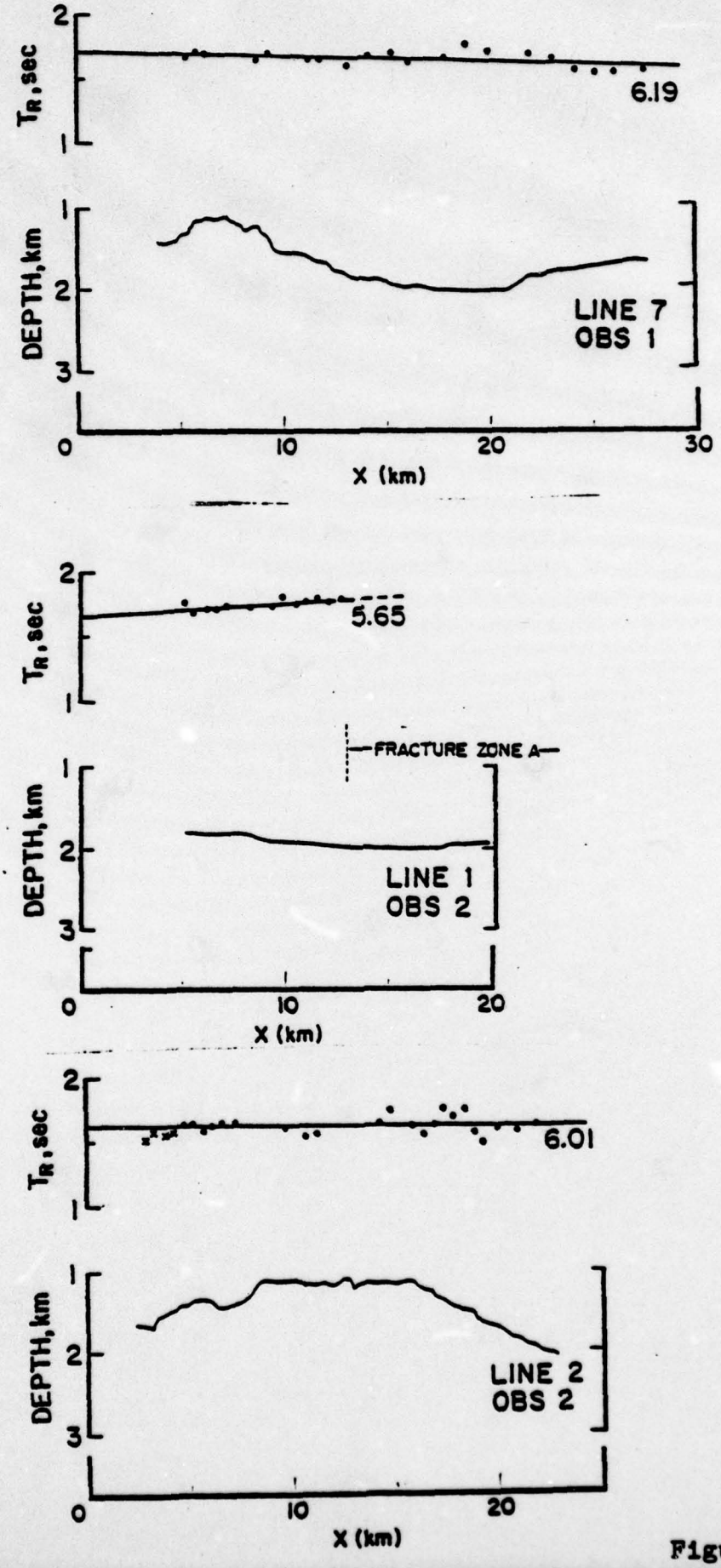

Figure 5 (cont.)

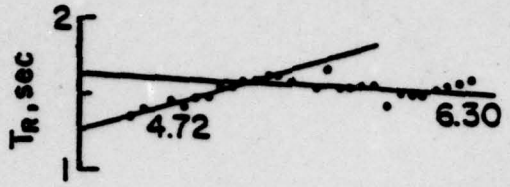

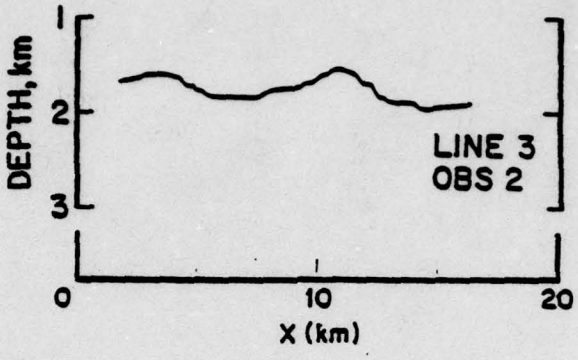

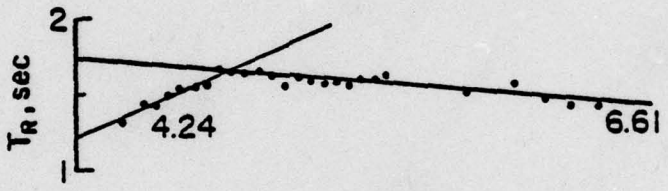

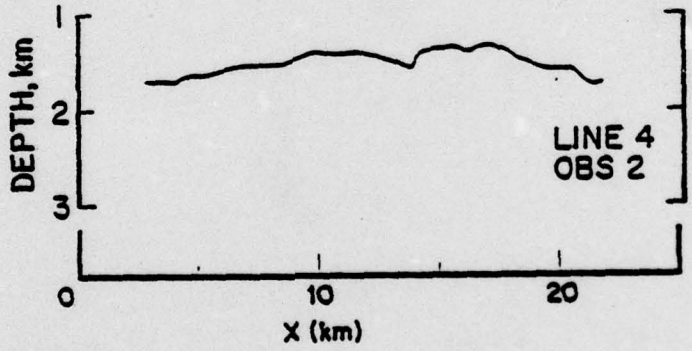

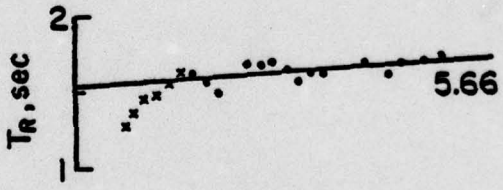

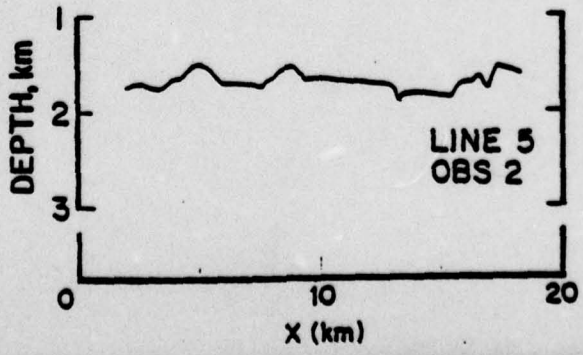

Figure 5 (cont.)

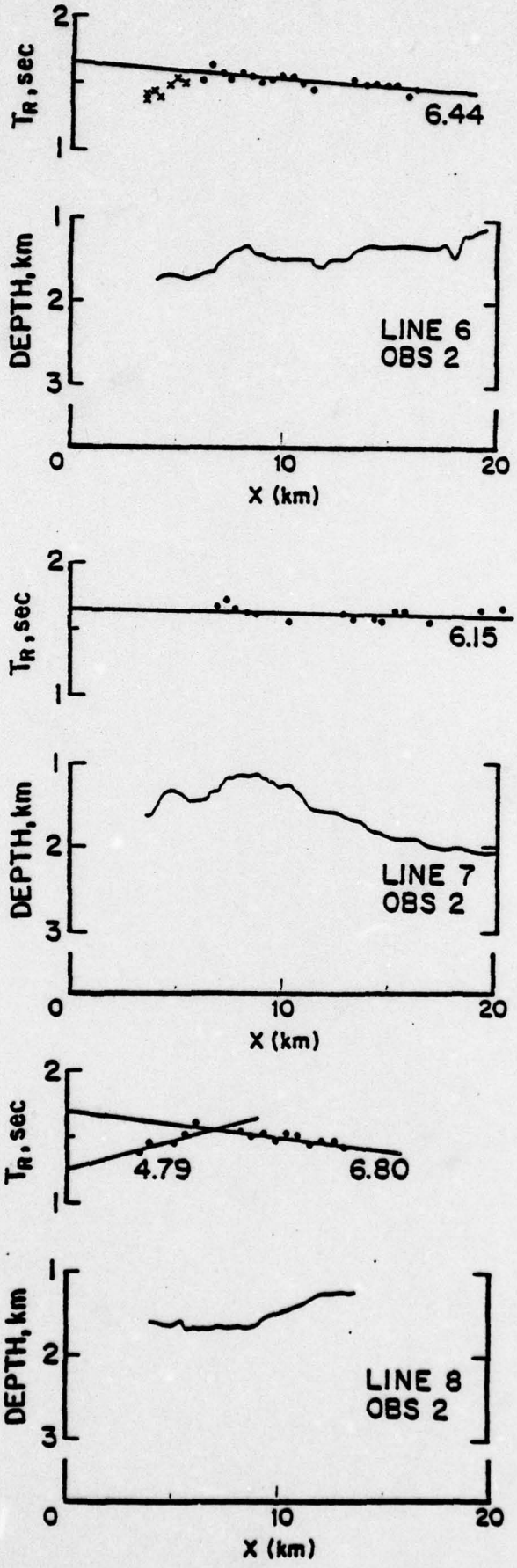

Figure 5 (cont.)

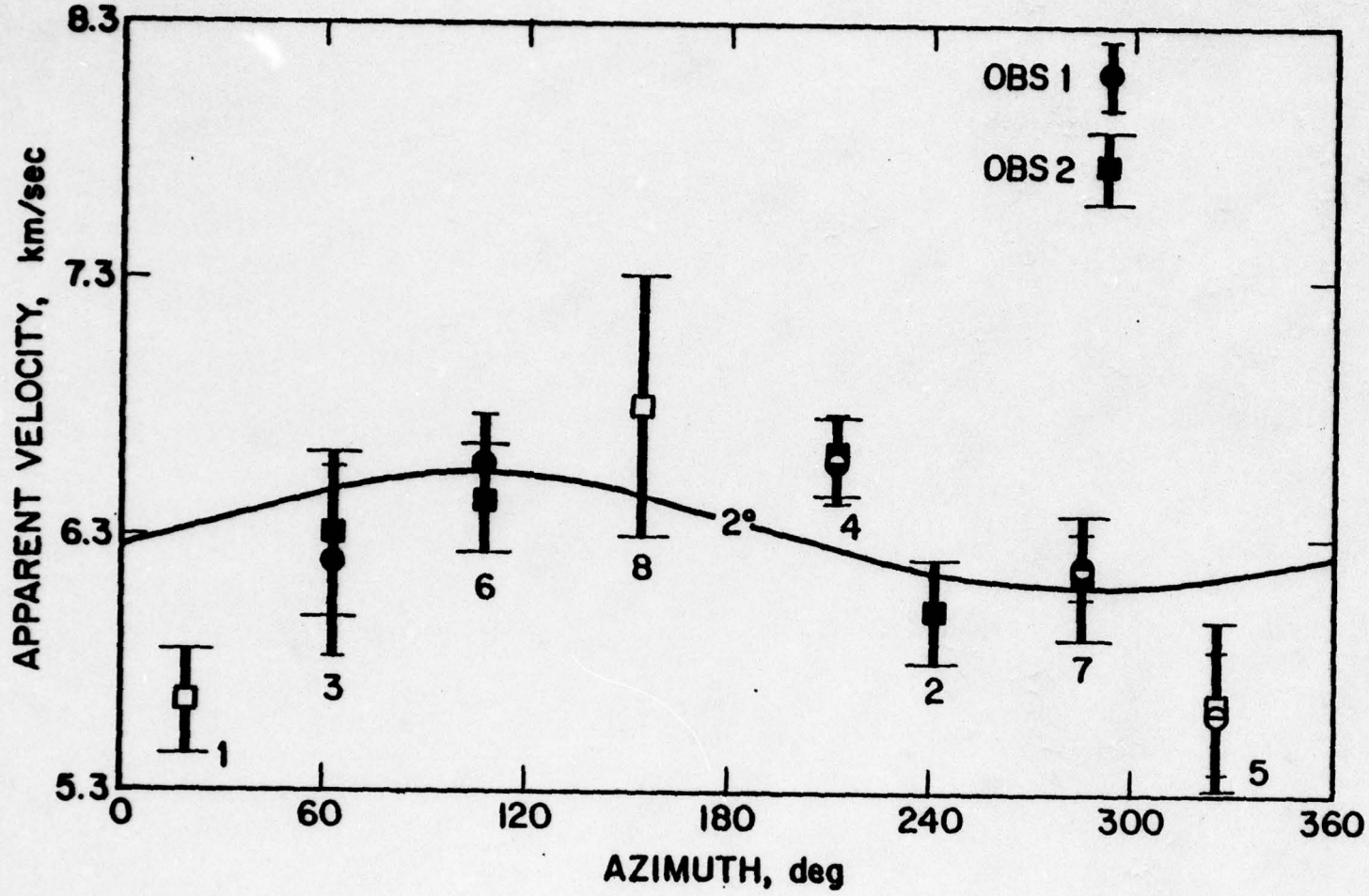
8.3
7.3
6.3
5.3
APPARENT VELOCITY, km/sec
OBS 1
OBS 2
2°
1
3
6
8
4
2
7
5
0
60
120
180
240
300
360
AZIMUTH, deg

Figure 6

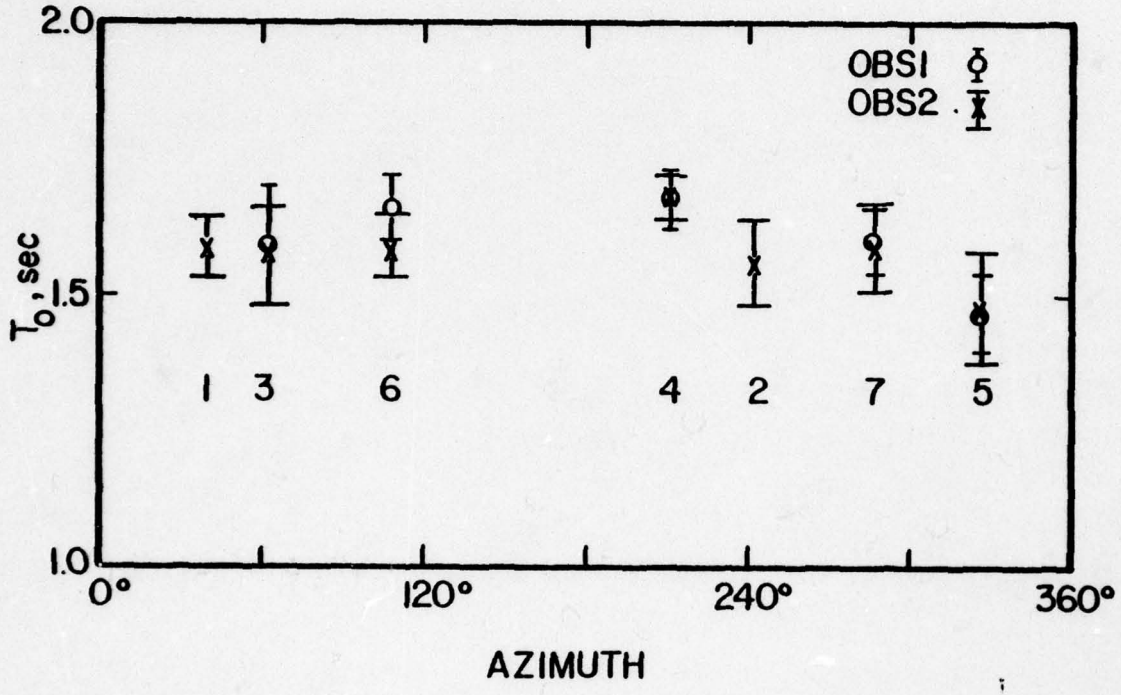

Figure 7

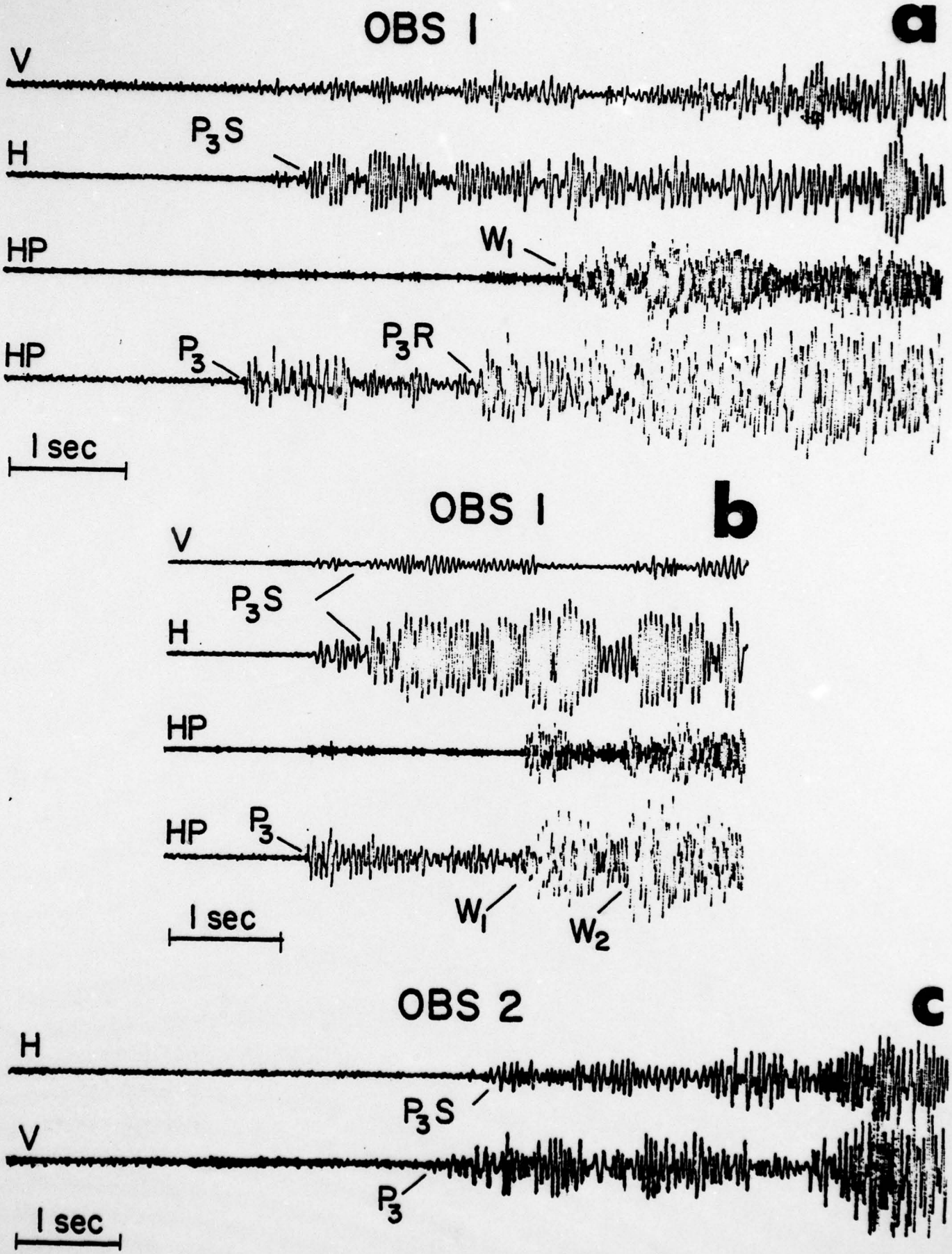
OBS 1
a
V
H
HP
HP
P_3S
W_1
P_3
P_3R
1 sec
OBS 1
b
V
H
HP
HP
P_3S
P_3
W_1
W_2
1 sec
OBS 2
c
H
V
P_3S
P_3
1 sec

Figure 8

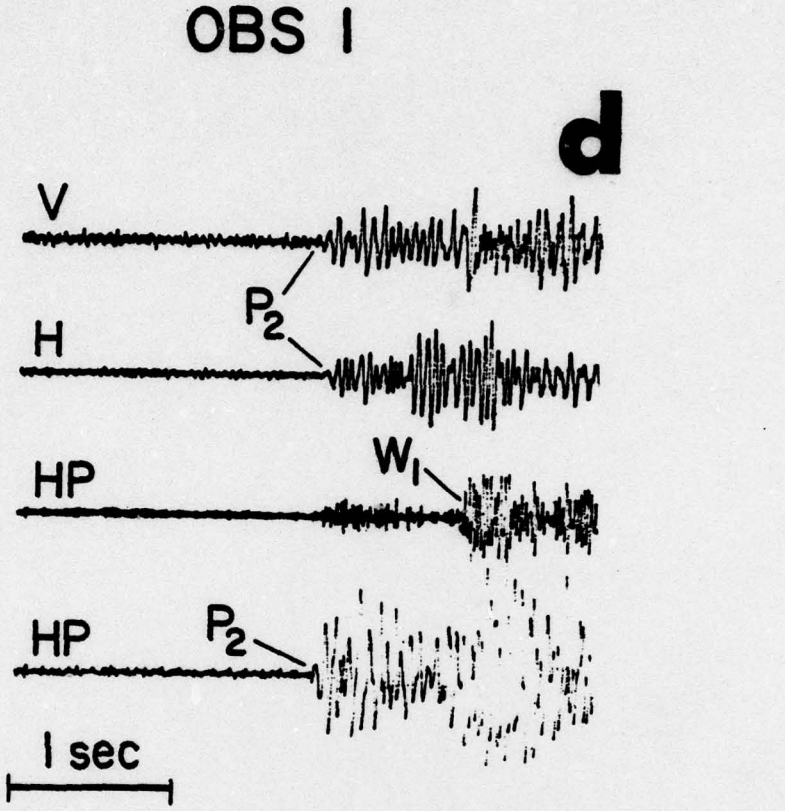

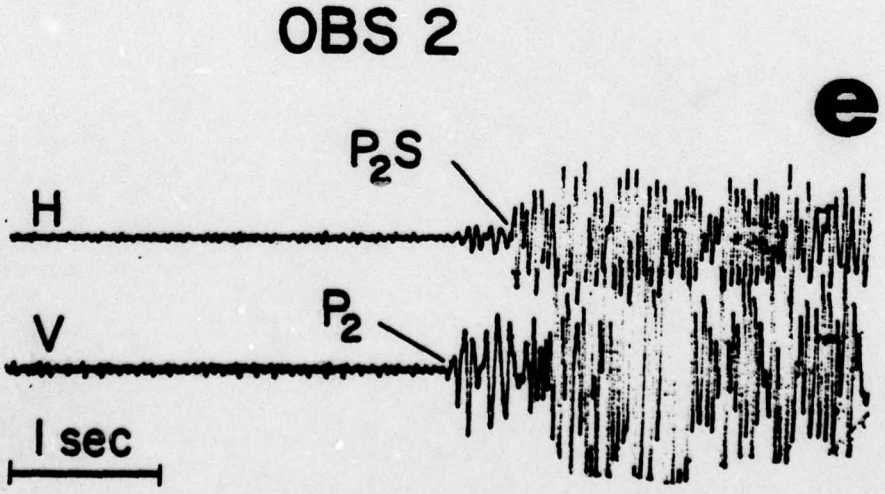

Figure 8 (cont.)

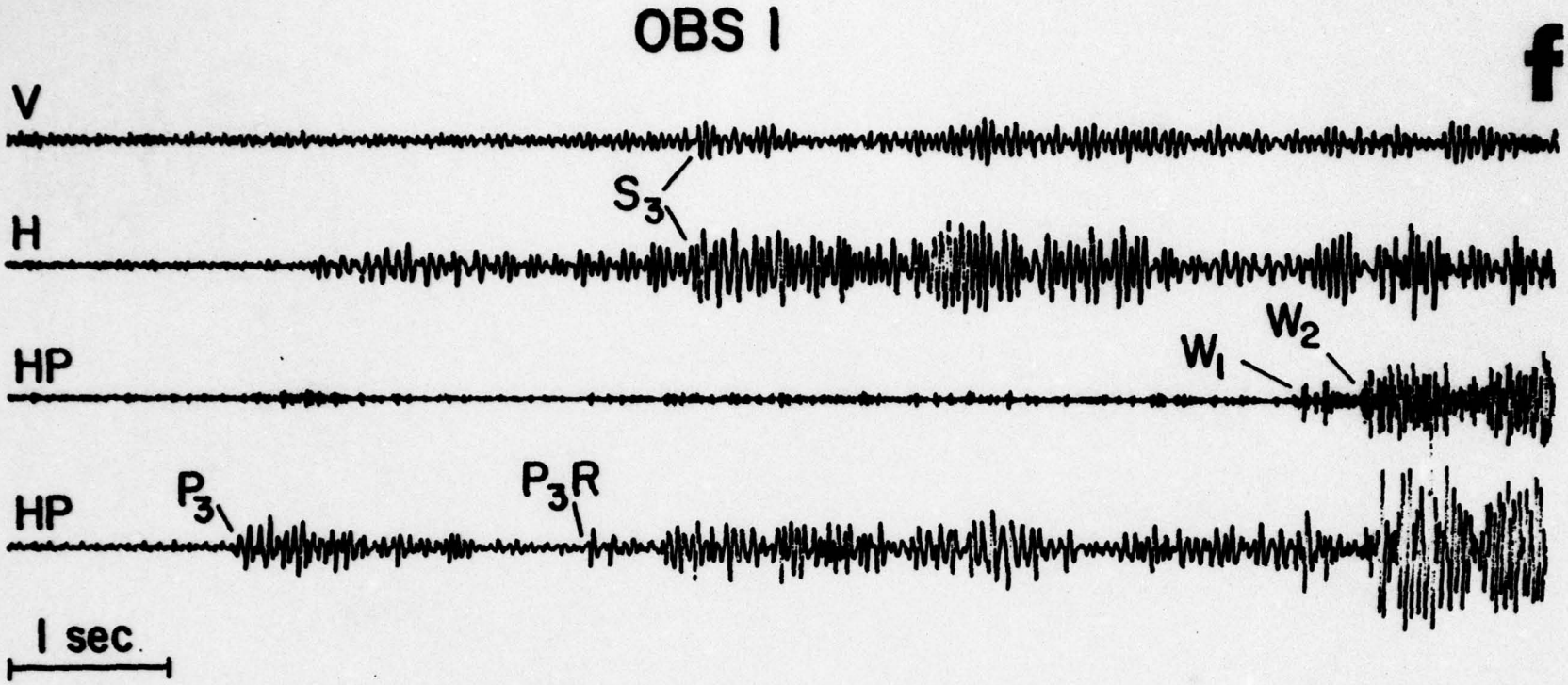

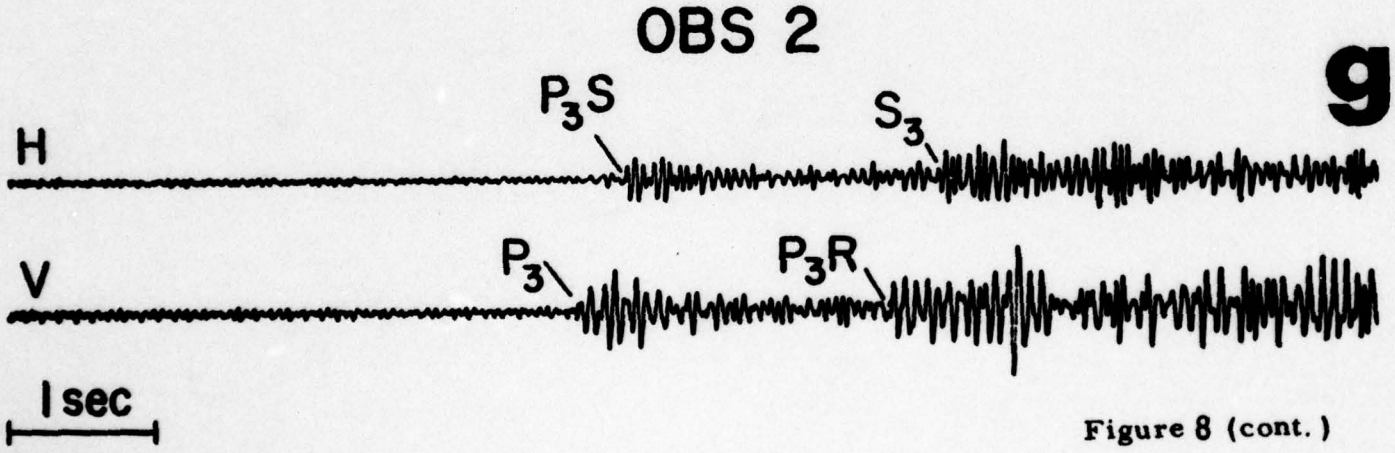

Figure 8 (cont.)

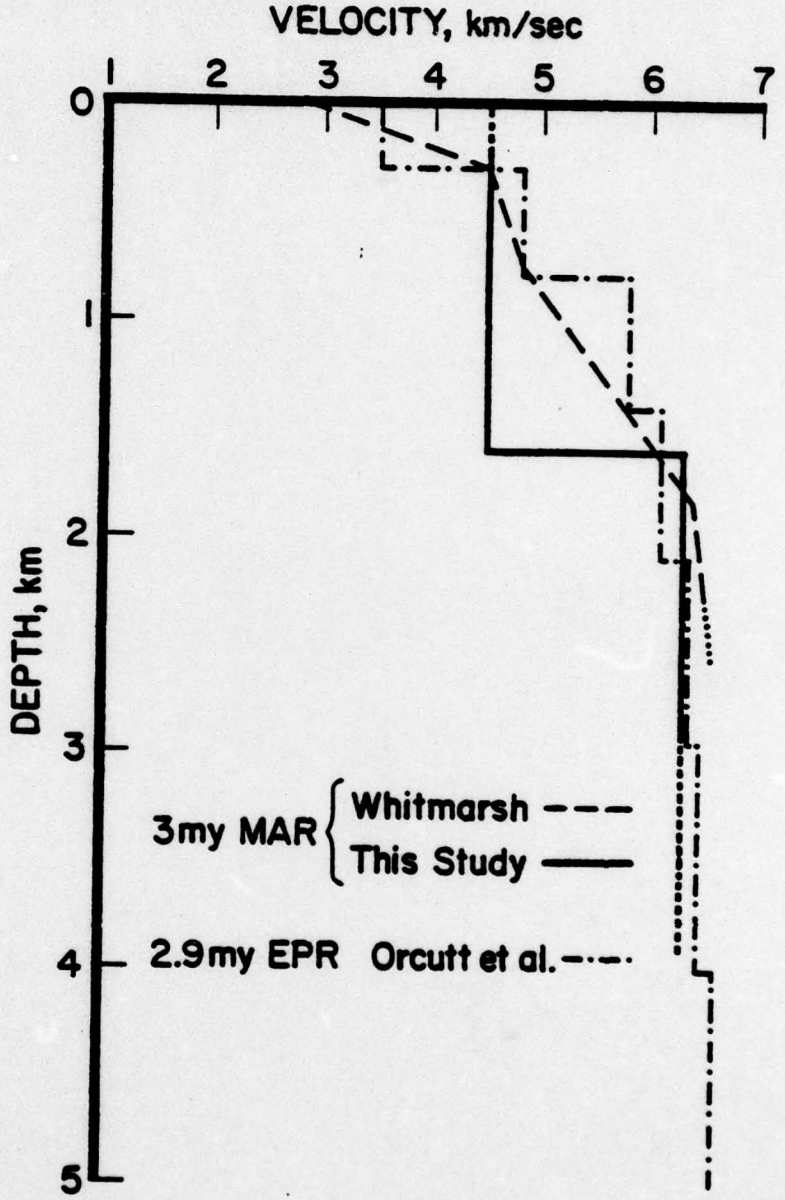
VELOCITY, km/sec
1
2
3
4
5
6
7
0
1
2
3
4
5
DEPTH, km
3my MAR
Whitmarsh
This Study
2.9my EPR Orcutt et al.

Figure 9

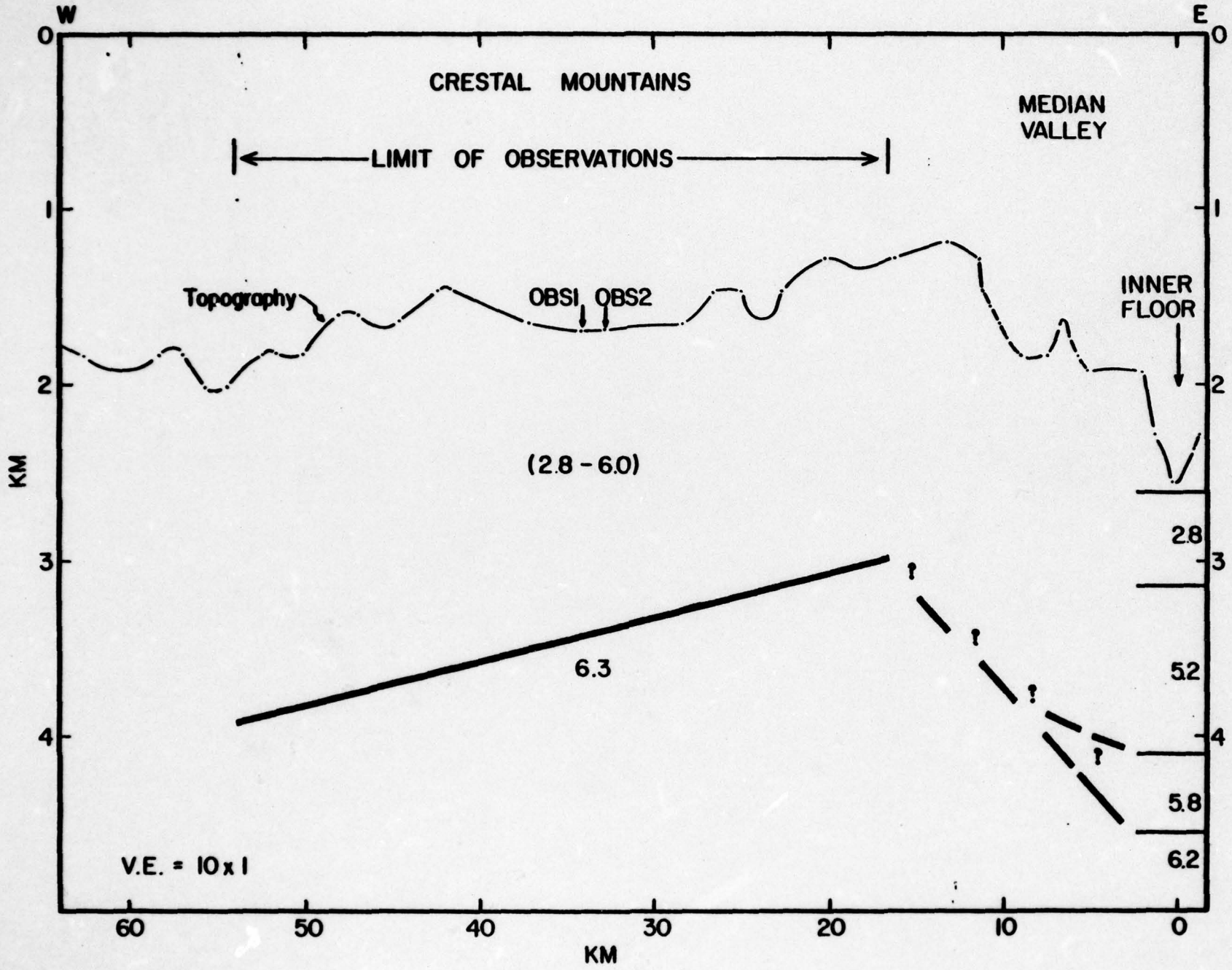
W
E
CRESTAL MOUNTAINS
MEDIAN VALLEY
LIMIT OF OBSERVATIONS
Topography
OBS1
OBS2
INNER FLOOR
(2.8 - 6.0)
6.3
2.8
5.2
5.8
6.2
V.E. = 10 x 1
KM
KM
0
1
2
3
4
60
50
40
30
20
10
0

Figure 10

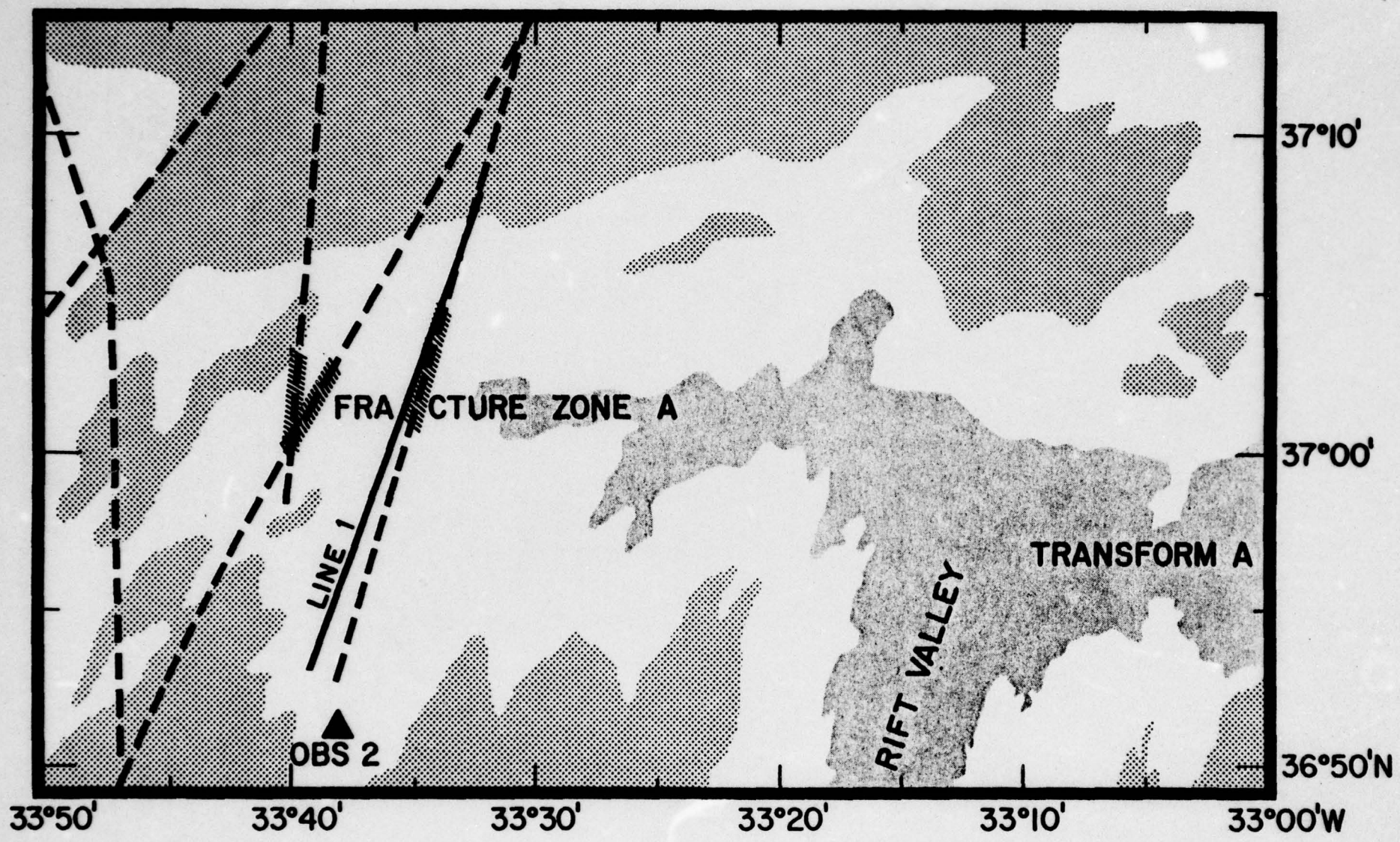
37°10'
37°00'
36°50'N
33°50'
33°40'
33°30'
33°20'
33°10'
33°00'W
FRACTURE ZONE A
LINE 1
OBS 2
RIFT VALLEY
TRANSFORM A
OBS REFRACTION LINE
V32-03 REFLECTION LINE
SEDIMENT FILLED TROUGH
>1200 FATHOMS
<900 FATHOMS
0
5
10
15km

Figure 11

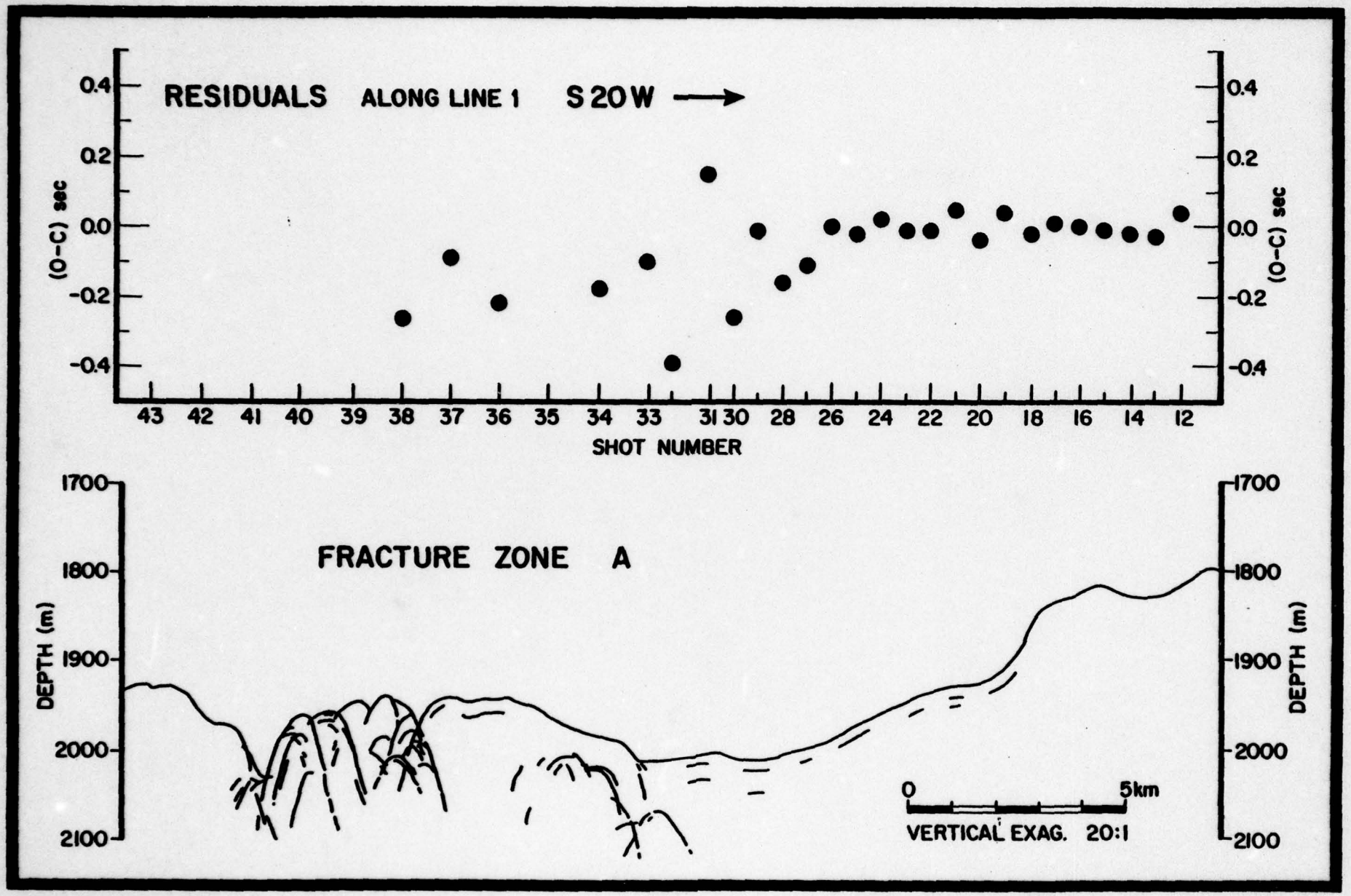
RESIDUALS ALONG LINE 1 S 20 W
0.4
0.2
0.0
-0.2
-0.4
(O-C) sec
43 42 41 40 39 38 37 36 35 34 33 31 30 28 26 24 22 20 18 16 14 12
SHOT NUMBER
FRACTURE ZONE A
1700
1800
1900
2000
2100
DEPTH (m)
0
5km
VERTICAL EXAG. 20:1

Figure 12

APPENDIX

Seismograms

In Figure 8 we present representative seismograms of the refracted arrivals. Seismograms of OBS 1 in Figure 8b show representative P_3 arrivals with clear onsets on the hydrophone trace at 5.8 km and 17.8 km. Although P_3 was not usually observed as an arrival with a clear onset on the vertical trace, it can be seen in Figure 8g (OBS 2) that with adequate charge size (2.95 kg at 15.2 km) P_3 has a clear onset.

The phase P_2, observed on all components, was usually an impulsive, large-amplitude arrival (Figure 8d and 8e) on the hydrophone and vertical traces. The impulsive phase permitted well-determined travel times, but the small interval of ranges at which P_2 appears as a first arrival, 3 km at the most, and no observable secondary arrivals beyond the crossover with P_3 did not permit as precise a determination of the apparent velocity of P_2 as of P_3.

A multiple of P_3, P_3R, is detected by the vertical and hydrophone traces (Figures 8a, 8f and 8g). This phase, probably reflected at the surface of the sea near the receiver, has been identified by Whitmarsh [1975] as G_1'.

Shear waves, S_3, are observed primarily on the horizontal component at ranges from 6.5 to 28 km on three of the shooting lines. The apparent velocities of this phase identify it as refracting with grazing incidence within the same layer as P_3. The onset of S_3 (see Figures 8f and 8g) is emergent and usually obscured by high signal levels and interference of earlier phases such as P_3R. The standard

error of reading S_3 is about 0.08 to 0.1 sec. As the seismograms of Figure 8 show, S_3 is identified primarily on the horizontal trace. This was true in general for this experiment. Improved recording and identification of refracted shear arrivals by bottom receivers requires the use of orthogonal sets of horizontal geophones.